Journal of Medicinal Chemistry

pubs.acs.org/jmc Article

Structure-Based Design of Selective LONP1 Inhibitors for Probing *In Vitro* Biology

Laura J. Kingsley,* Xiaohui He, Matthew McNeill, John Nelson, Victor Nikulin, Zhiwei Ma, Wenshuo Lu, Vicki W. Zhou, Mari Manuia, Andreas Kreusch, Mu-Yun Gao, Darbi Witmer, Mei-Ting Vaillancourt, Min Lu, Sarah Greenblatt, Christian Lee, Ajay Vashisht, Steven Bender, Glen Spraggon, Pierre-Yves Michellys, Yong Jia, Jacob R. Haling, and Gérald Lelais*

Cite This: *J. Med. Chem.* 2021, 64, 4857−4869 Read Online

ACCESS | Metrics & More | Article Recommendations | Supporting Information

ABSTRACT: LONP1 is an AAA+ protease that maintains mitochondrial homeostasis by removing damaged or misfolded proteins. Elevated activity and expression of LONP1 promotes cancer cell proliferation and resistance to apoptosis-inducing reagents. Despite the importance of LONP1 in human biology and disease, very few LONP1 inhibitors have been described in the literature. Herein, we report the development of selective boronic acid-based LONP1 inhibitors using structure-based drug design as well as the first structures of human LONP1 bound to various inhibitors. Our efforts led to several nanomolar LONP1 inhibitors with little to no activity against the 20S proteasome that serve as tool compounds to investigate LONP1 biology.

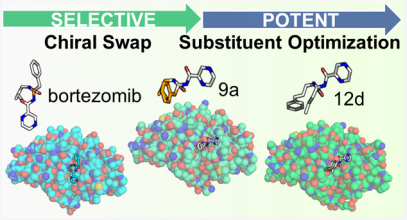

INTRODUCTION

LONP1 is a mitochondrial serine protease that is widely conserved across eukaryotic species. LON proteases along with ClpXP, ClpAP, ClpCP, HslUV, FtsH, and PAN/20S make up the AAA+ (ATPase associated with diverse cellular activities) family of proteases.[1] This family of proteases is responsible for maintaining cellular homeostasis by removing unwanted or damaged proteins within the cell.[2−4] As the name suggests, each member of this family contains at least one AAA+ domain, which utilizes ATP as an energy source to unfold substrate proteins. AAA+ proteases function as multimers, forming barrel-like structures through which target proteins are forcibly threaded prior to degradation.[1,5−7] While physical seclusion of the active site in AAA+ proteases provides some level of control, substrate selection and regulation of AAA+ proteases are still poorly understood.[2]

Recent structural studies on the LON family member, LonA, have provided some insights into the structure, function, and regulation of the LON proteases. The LON proteases function as homo-hexamers in which each individual protein unit contains both the ATPase and protease functions.[1] This contrasts with other family members where the ATPase and protease functions are found in different protein units. In LON proteases, the protease domain linker connects the ATPase to the protease domain and is thought to be critical for substrate unfolding as it allows for a large, ATP-driven conformational change that pulls substrate proteins into the protease active site.[8] Studies have indicated that in the bacterial MtaLonA, Mg^{2+} is a key cofactor for LONP1 activation.[9] Additionally, a disulfide-controlled redox switch is thought to modulate LON activity by controlling the exit pore size; however, these key cysteines are not conserved in human LON proteases suggesting alternative regulation mechanism(s).[6,10]

While the regulatory mechanisms of LON proteases, including LONP1, are not fully understood, it is clear that dysregulation of LONP1 leads to disease. Genetic studies have found that, although rare, mutations that impair the function of LONP1 lead to severe developmental complications in the cerebral, ocular, dental, auricular, and skeletal systems known as CODAS syndrome and other mitochondrial diseases.[11,12] Conversely, recent studies suggest that elevated expression of LONP1 plays a pro-tumorigenic role in several cancers including colorectal, cervical, and melanoma cancers.[13−15]

Despite a growing understanding of the complex regulatory mechanisms of LONP1 and its importance in various disease states, LONP1-specific tool compounds are lacking. Most studies to date have relied on a limited set of non-selective LONP1 tool compounds including oleanane 2-cyano-3,12-dioxooleana-1,9-dien-28-oic acid and its derivatives, (−)-ses-amin, obtusilactone A, and bortezomib.[4,16] Furthermore, homozygous LONP1 knockouts are embryonically lethal, making it difficult to study the biological effects of a complete lack of LONP1.[14,17] While silencing approaches have been used to help elucidate the roles of LONP1,[18] they are often

Received: December 23, 2020
Published: April 6, 2021

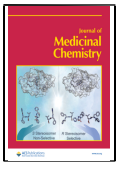

https://doi.org/10.1021/acs.jmedchem.0c02152
J. Med. Chem. 2021, 64, 4857−4869

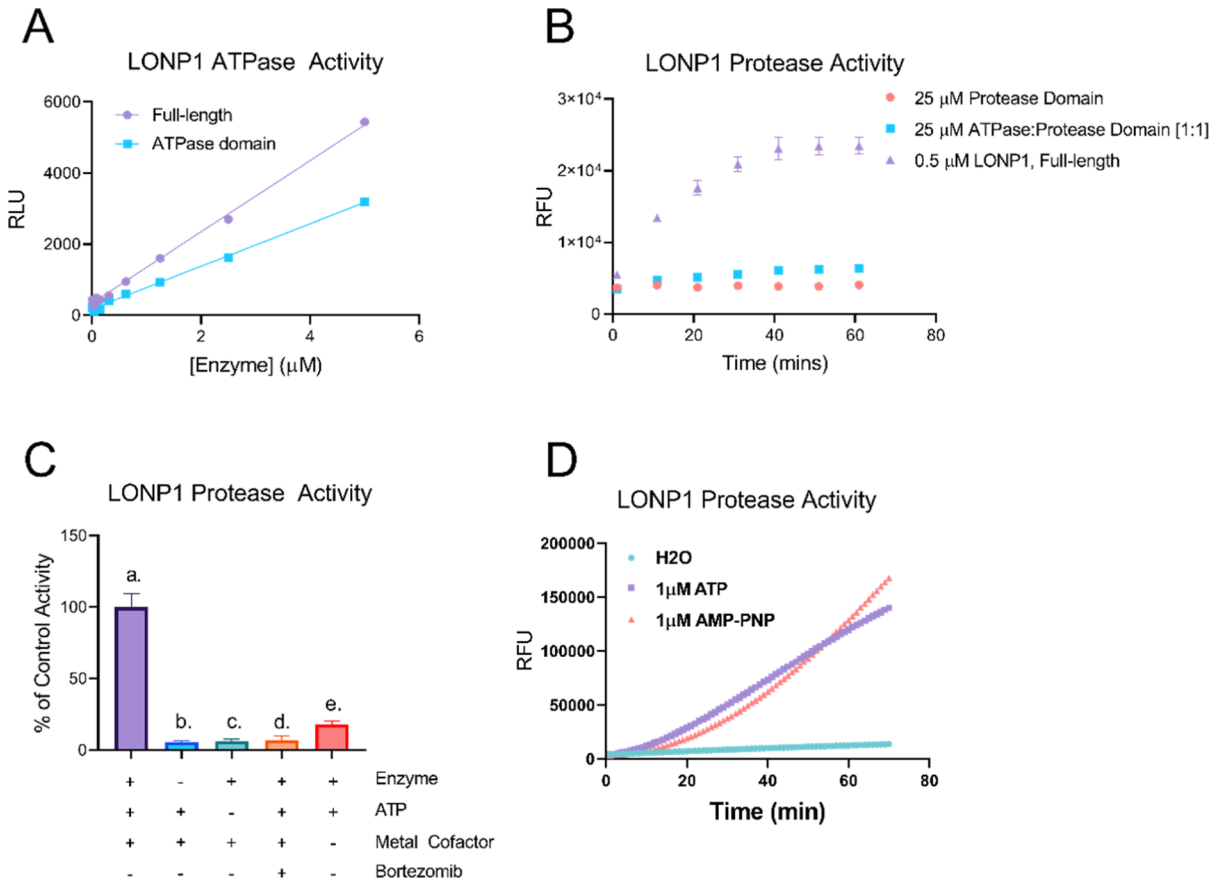

Figure 1. Biochemical characterization of human LONP1. (A) ATPase activity determination of LONP1 full-length protein and ATPase domain-only construct (a.a. 408−752) using the ADP-Transcreener assay. (B) Protease activity determination of LONP1 full-length protein (triangles), protease domain-only construct (a.a 754−959) (circles), and mixture of ATPase domain and protease domain at 1:1 ratio (squares) using the LONP1 protease assay. (C) Full-length LONP1 characterization under various conditions: (a) in the presence of all components (defined as 100% control activity); (b) in the absence of enzyme (defined as background); (c) in the absence of ATP; (d) in the presence of excess bortezomib (10 μM; 55-fold above its IC_{50}); and (e) in the absence of metal cofactor ($CaCl_2$). (D) Kinetics of LONP1 activation in the presence of either 1 μM ATP or 1 μM AMP-PNP.

challenging to implement.[19] Coupling genetic strategies to pharmacological intervention can both offer deeper insights and pave the way for therapeutic strategy development. Recently, the importance of "probe" compounds has been highlighted in the literature as necessary to understand biology.[20] Herein, we report our efforts toward better understanding the structure−function relationships in LONP1 inhibition and the identification of specific LONP1 inhibitors that can be used to dissect the LONP1 biological function in cancer and other diseases.

RESULTS AND DISCUSSION

Characterization of LONP1 Domains. To understand the cross-regulation between the ATPase and the protease domains of LONP1, we first studied the two domains independently. The ATPase domain (a.a. 408−752) alone retained ∼60% of ATPase activity compared to the full-length LONP1 (Figure 1A); in contrast, the protease domain alone (a.a. 754−959) was devoid of proteolytic activity, even when tested at 50-fold higher concentration than full-length LONP1 (Figure 1B). We then attempted to reconstitute "full-length" LONP1 protease activity in trans by mixing the ATPase and protease domains at a 1:1 ratio, but this reconstituted protein demonstrated only minimal protease activity (0.14% of full-length LONP1 activity; Figure 1B). Our findings indicate that the protease activity is dependent on the AAA+ domain ATPase activity, but not vice versa, and the protease domain linker that connects the ATPase to the protease domain is critical for this intramolecular domain regulation.

To further understand the effect of ATPase domain on protease activity, we tested full-length LONP1 under various conditions. The protease activity was completely abolished in the absence of ATP (Figure 1C(c)) similar to the effect of full protease inhibition by bortezomib (10 μM; 55-fold above its IC_{50}; Figure 1C(d)). However, when the metal cofactor was removed while keeping ATP in the assay mixture, residual protease activity was observed (Figure 1C(e)), indicating that there exists a non-ATPase-dependent protease activity requiring binding of ATP to LONP1. To test if nucleotide binding, rather than hydrolysis, is necessary for protease activity, AMP-PNP was titrated into the LONP1 protease assay in the presence of 1 μM ATP. Interestingly, we observed a dose-dependent increase in LONP1 activation (Figure S1), suggesting that binding alone to the ATP site is capable of promoting some protease activity. To confirm this, we replaced ATP with AMP-PNP in the assay. In the absence of both ATP and AMP-PNP, no protease activity was detected. On the other hand, AMP-PNP (1 μM, equivalent to ATP concentration used in the assay) was able to fully rescue the protease activity of LONP1, even though the kinetics of the two

https://doi.org/10.1021/acs.jmedchem.0c02152
J. Med. Chem. 2021, 64, 4857−4869

Scheme 1. Preparation of Analogues Following Known Synthetic Procedures[26−32] *a*

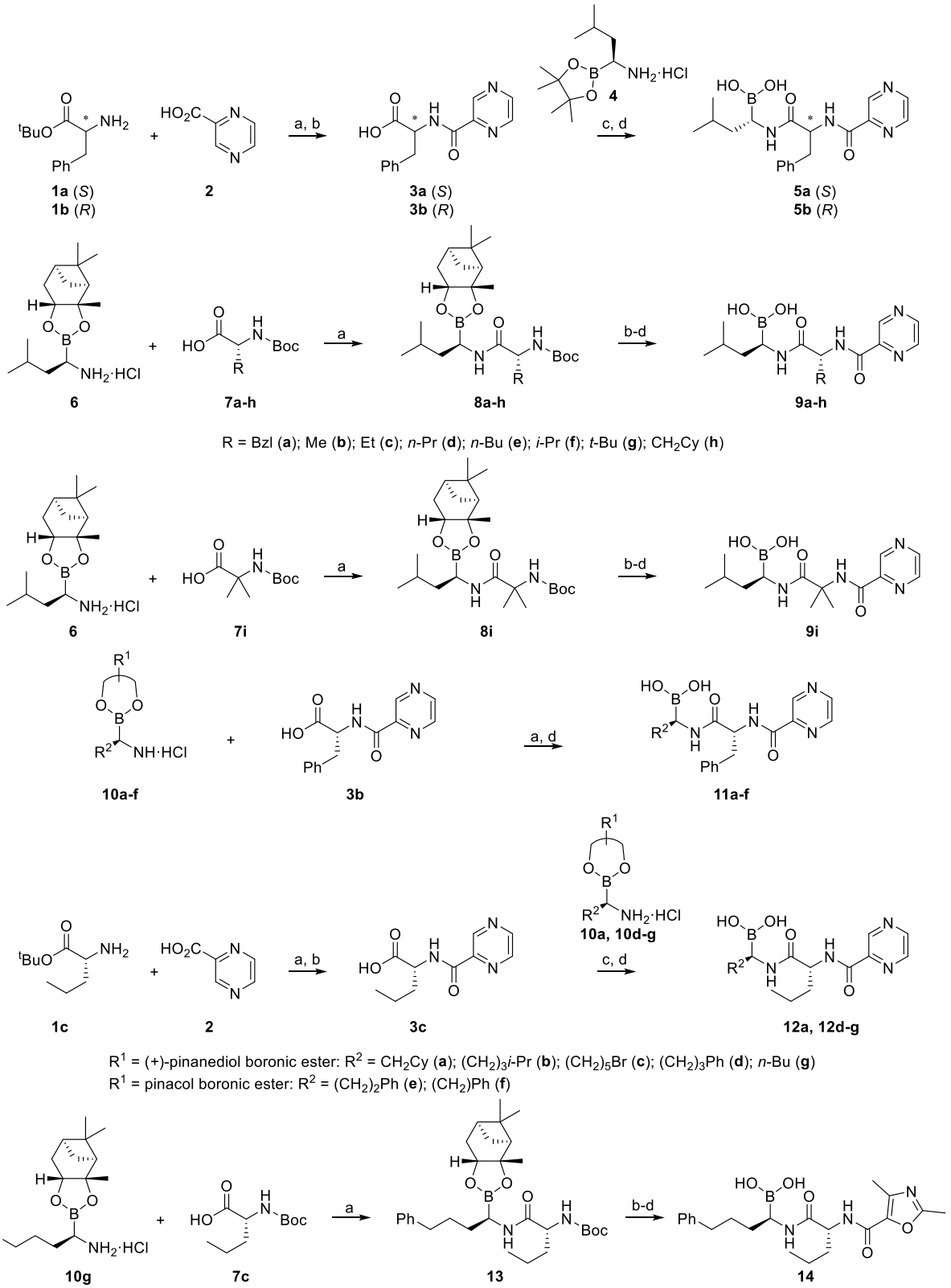

[a]Reagents and conditions: (a) DIPEA, HATU, DMF or DCM, and −15 °C to room temperature. (b) HCl/dioxane. (c) For **5a−b**: **4**, TBTU, DIEA, DCM, and −15 °C to room temperature. For **9a−i**: **2**, HATU, DIPEA, DMF or DCM, and −15 °C to room temperature. For **12a** and **12d−g**: **10a** or **10d−g**, HATU, DIPEA, DMF or DCM, and −15 °C to room temperature. For **14**: 2,4-dimethyloxazole-5-carboxylic acid, HATU, DIPEA, DCM, and −15 °C to room temperature. (d) Isobutyl boronic acid, HCl, and heptane/MeOH.

https://doi.org/10.1021/acs.jmedchem.0c02152
J. Med. Chem. 2021, 64, 4857−4869

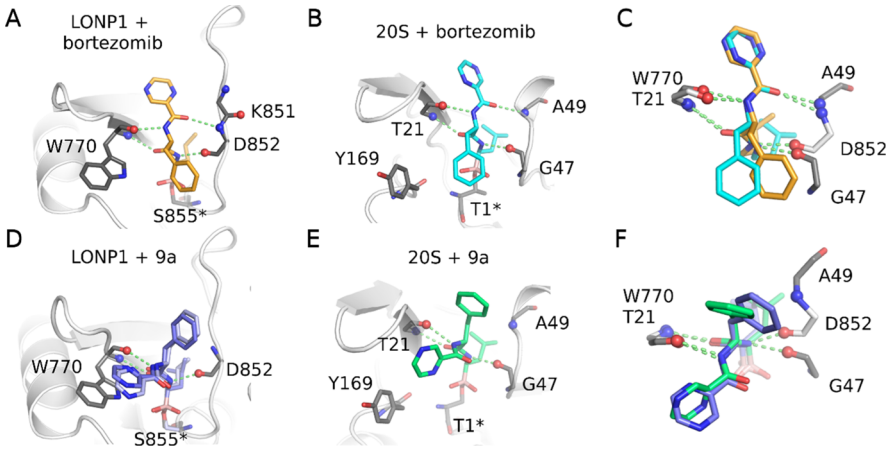

Figure 2. Binding site comparison of LONP1 and the 20S proteasome β5-subunit. Hydrogen bonds to the protein backbones are shown in green and the reactive serine or threonine residues for LONP1 and 20S proteasome, respectively, are indicated by an asterisk (*). (A) Bortezomib bound to human LONP1 protease domain (PDB ID 6X27). (B) Bortezomib bound to the β5 site of the human 20S proteasome (PDB ID 5LF3). (C) Comparison of the binding mode of bortezomib in LONP1 (yellow) vs the 20S proteasome β5 site (cyan). (D) Crystal structure of **9a** bound to LONP1 (dark purple; PDB ID 6WZV) and docked pose (light purple). The root-mean-square deviation (RMSD) between the docked and crystal pose is 0.63. (E) Docking model of **9a** bound to the β5 subunit of the human 20S proteasome. (F) Overlay of the crystal pose of **9a** bound to LONP1 (purple; PDB ID 6WZV) with the predicted binding mode in the β5 subunit of the human 20S proteasome (green).

reactions were very different. Instead of showing a linear kinetic similar to ATP, a lag phase was observed for AMP-PNP (Figure 1D), indicating that binding of AMP-PNP likely induces a large conformational change of the protein, priming the protease domain into an active conformation for substrate degradation. These results suggest that ATP (or its analogues) occupying the ATP site, not the ATPase activity itself, is necessary for the protease activity of LONP1. Thus, from a drug discovery perspective, our results indicate that a protease inhibitor, but not an ATPase inhibitor, will be most effective for LONP1 inhibition. Our findings are consistent with what was described for prokaryotic evolutionarily conserved LonA from *Meiothermus taiwanensis*.[9,21]

Assay Design, Primary Hit Identification, and Chemistry. Our strategy for identifying selective LONP1 protease site inhibitors started with a comprehensive high-throughput screening (HTS) of the Novartis compound library using recombinant hexameric LONP1. The LONP1 biochemical assay was modified based on the assay reported by Fishovitz *et al.*[22] In brief, the LONP1 HTS assay measures activity via cleavage of a substrate peptide. Initially, the substrate peptide is intramolecularly quenched, but cleavage by LONP1 results in the release of fluorescent fragments. Compound inhibition of LONP1 prevents peptide cleavage and therefore leads to a reduction in a fluorescent signal. Compounds were screened at a single-point concentration in a 1536-well format. The screen quality was high with a Z'-factor of 0.6. Compounds were designated as hits if the percent inhibition exceeded 3 standard deviations from the mean activity. The hit rate was 1.16%. Hits were confirmed using a 12-point dose response in the same assay.

Boronic acid peptides were identified as one of the top series in the HTS. The members of this series, including bortezomib and ixazomib, have been previously reported to have nanomolar activity against two of the three subunits of the 20S proteasome and also LONP1 from various source organisms.[9,23−26] A medicinal chemistry campaign was initiated to develop a bortezomib analogue devoid of 20S proteasome activity and identify tool compounds useful for investigating LONP1 biology. The analogues were prepared following known synthetic procedures (Scheme 1).[26−28] Two routes were used: on the one hand, amino acid tertbutyl esters (**1a−c**) were first acylated with pyrazine-2-carboxylic acid (**2**), then coupled with amino boronate esters, previously prepared through known procedures,[29−32] and the resulting boronic esters were deprotected to afford the desired compounds (**5a−b**, **11a−f**, **12a**, and **12d−g**). Alternatively, Boc-protected amino acids were first coupled with amino boronate esters, Boc-deprotected, and coupled with the appropriate heteroaryl carboxylic acids before final boronate ester deprotection to afford the corresponding LONP1 inhibitors (**9a−i** and **14**).

Conserved Backbone Interactions Contribute to Lack of Specificity for Bortezomib. To better understand the structure−activity relationship (SAR) of bortezomib in the context of LONP1 specificity, we co-crystallized bortezomib with the LONP1 protease domain (PDB ID 6X27, Figure 2A) and compared it to the previously reported[33] bortezomib-bound structure of the human 20S proteasome (PDB ID 5LF3, Figure 2B). For clarity, structural comparisons in the main text between LONP1 and the 20S proteasome will refer specifically to the chymotrypsin-like (β5) site as it has the highest affinity for bortezomib;[34] however, comparisons to the caspase (β1) and trypsin-like (β2) subunits can be found in the Supporting Information (Figure S2A,B). The overall sequence identity between LONP1 and the chymotrypsin-like (β5) subunit of the 20S proteasome is low, 15.1% (27.1% homology), as is the overall architecture of the bortezomib binding pocket. Of the residues lining the binding site, the conservation is even lower; only 4 of the 18 residues within 5 Å of the LONP1 protease binding site are roughly structurally conserved (Figure S2E).

Despite the structural and sequence differences within the LONP1 and chymotrypsin pockets, the binding affinity of bortezomib is similar between the two proteases (Table 1). One explanation for this may be that the binding interactions are congruous between the two proteases (Figure 2C). The reactive oxygen that forms a reversible covalent bond to the boronic acid group of bortezomib (S855 in LONP1 and T1 in the 20S proteasome) is spatially conserved in both species (Figure 2A,B, reactive residues indicated with *). Additionally, the primary contacts between bortezomib and the protein

https://doi.org/10.1021/acs.jmedchem.0c02152
J. Med. Chem. 2021, 64, 4857−4869

Table 1. Biochemical Activity Profiles of Bortezomib and Analogues in LONP1 and 20S Proteasome[a]

compound	LONP1	20S proteasome
bortezomib	0.183 ± 0.150	0.097 ± 0.072
5a	2.111 ± 0.129	1.524 ± 0.268
5b	2.980 ± 0.134	1.701 ± 0.235
9a	0.253 ± 0.161	>10
9b	0.433 ± 0.161	2.676 ± 0.905
9c	0.408 ± 0.212	>10
9d	0.187 ± 0.092	>10
9e	0.093 ± 0.036	>10
9f	0.546 ± 0.258	3.971 ± 4.608
9g	2.850 ± 0.632	>10
9h	0.137 ± 0.077	0.843 ± 0.182
9i	6.199 ± 0.032	n.d.
11a	0.092 ± 0.015	0.541 ± 0.582
11b	0.065 ± 0.013	1.036 ± 0.490
11c	0.077 ± 0.020	1.943 ± 0.938
11d	0.018 ± 0.004	0.259 ± 0.194
11e	0.034 ± 0.015	0.262 ± 0.051
11f	0.109 ± 0.032	0.679 ± 0.227
12a	0.136 ± 0.134	>10
12d	0.017 ± 0.012	>10
12e	0.092 ± 0.054	>10
12f	0.556 ± 0.354	>10
12g	0.038 ± 0.010	>10
14	0.059 ± 0.046	>10

[a]HTRF IC_{50} values (μM) were determined after a 1 h compound treatment. All data are an average of at least duplicate measurements.

backbone are maintained (Figure 2A–C). These conserved interactions result in a similar binding pose of bortezomib in LONP1 and the 20S proteasome and likely explain the similar affinity in the two proteases (Figure 2C). An alternate conformation for the P2 benzyl moiety of bortezomib was observed in the LONP1–bortezomib co-structure (PDB 6X27) and modeled for all chains but B, with refined occupancies of 0.36–0.45.

Stereochemical Inversion at the P2 Position Improves Selectivity by Reducing the Potency on 20S Proteasome. Among the bortezomib analogues included in the Novartis library, there were indications that stereochemistry could impact activity on both LONP1 and 20S proteasome (data not shown). For this reason, we prepared the bortezomib diastereomers **5a–b** and **9a** and assessed their activity in both targets (Table 1). Inverting the boron stereocenter (referred as P1 in this paper; **5a**) or converting both bortezomib stereocenters (**5b**) had detrimental effect on LONP1 and 20S proteasome. In contrast, conversion of the amino acid stereocenter (referred as P2 position herein) to *R* (**9a**) resulted in more than 100-fold reduction in potency toward the 20S proteasome, with only a slight drop in potency toward LONP1 (Table 1).

To rationalize the observed improvement in selectivity and relative changes in potency, we developed a series of docking models for both LONP1 and the 20S proteasome. For both proteases, the models predict an alternative binding conformation wherein the orientation of the P2 and P3 substituents is switched due to the stereoinversion at the P2 site (Figure 2D–F). In the 20S proteasome, the alternative conformation of **9a** results in the weakening and loss of H-bonds from the P3 amide (Figure 2E) and also shifts the P2 benzyl group out of the pocket toward the solvent. Docking of **9a** to LONP1 (Figure 2D, light purple) suggested the same weakening and loss of the H-bonds from the P3 amide; however, in LONP1, the pyrazine ring of P3 forms a π–π stack with W770 of LONP1, as was later confirmed by crystallography (Figure 2D, dark purple, PDB ID 6WZV, ligand RMSD = 1.1). Additional density for the **9a** co-structure with LONP1 was observed around the boronic acid but its identity could not be unambiguously confirmed. The

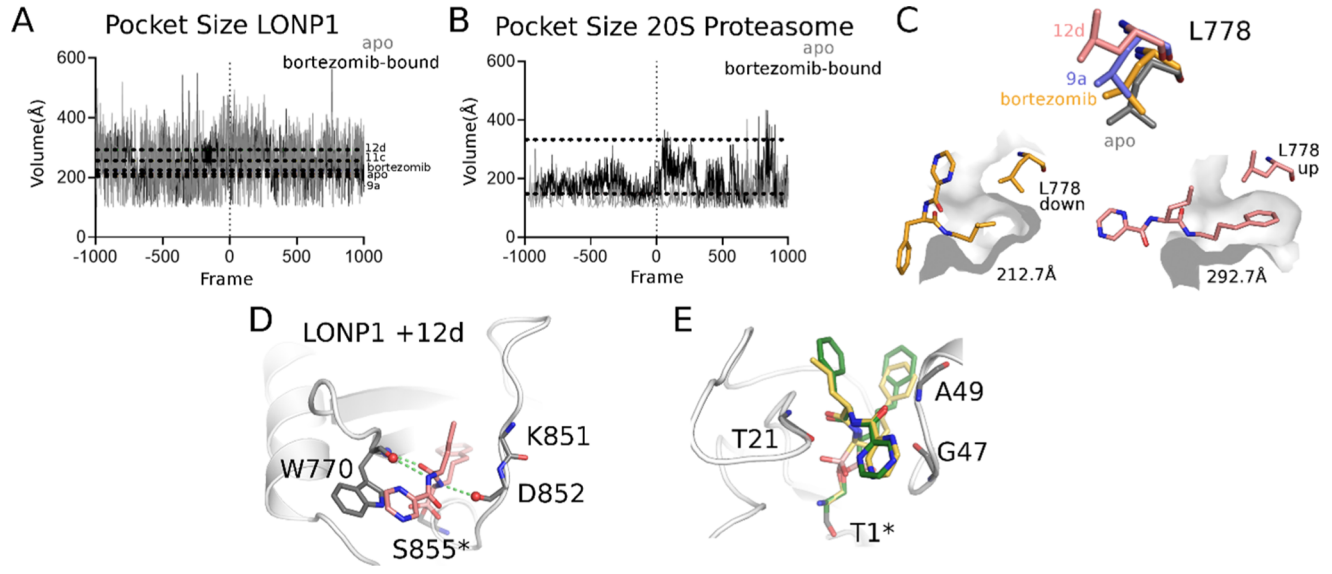

Figure 3. MD simulation and docking poses of LONP1 inhibitors with LONP1 and 20S proteasome. (A) Binding pocket dynamics over 200 ns of MD simulation of the apo- and bortezomib-bound LONP1 and (B) 20S proteasome β5 subunit. (C) Conformational states of L778 observed in LONP1 crystal structures (top panel; PDB IDs 6WYS, 6X27, 6WZV, and 6X1M). The interior pocket surface and volume are shown for the bortezomib-bound (PDB ID 6X27) and **12d**-bound (PDB ID 6X1M) crystal structures (lower panel). (D) Binding mode of **12d** in LONP1 displaying hydrogen bonds to the backbone and the π–π stacking with W770. (E) Predicted binding modes of **11d** (green) and **12d** (yellow) using the 20S proteasome-expanded pocket model.

https://doi.org/10.1021/acs.jmedchem.0c02152
J. Med. Chem. 2021, 64, 4857–4869

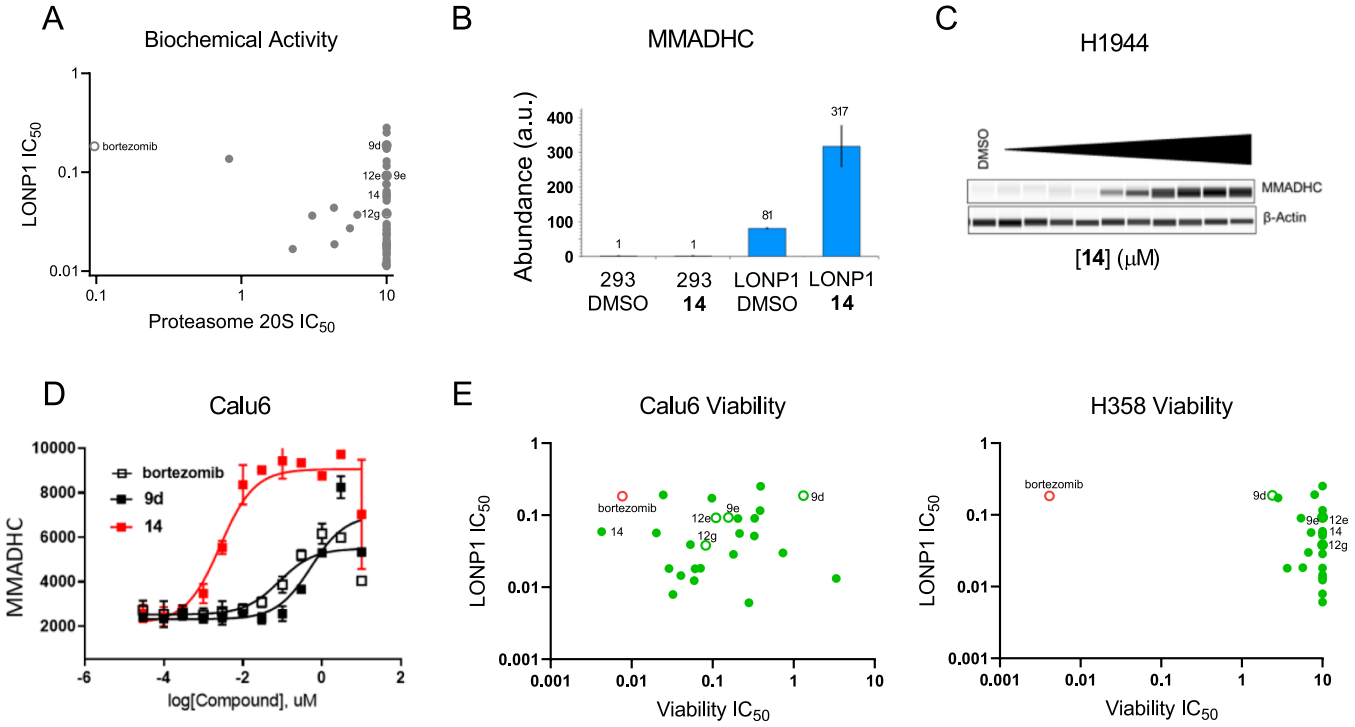

Figure 4. Biochemical and cellular activity of LONP1 inhibitors. Full circles represent P3 SAR of **12d**, while open circles represent a subset of compounds from Table 1. All scatter plot data at 10 μM IC_{50} correspond to compounds with IC_{50}s > 10 μM. (A) Scatter plot of LONP1 (*y*-axis) and 20S proteasome (*x*-axis) biochemical IC_{50}s. (B) Relative abundance of MMADHC following affinity purification and mass spectrometry analysis of cells treated with DMSO or **14**. Abundance ratios were calculated based on the label-free quantitation from MS1 intensity of precursor ions using Thermo Scientific Proteome Discoverer software version 2.4. (C) WES analysis of MMADHC in H1944 cells following treatment with a 1:3 serial dilution of **14** starting at 10 μM. (D) MMADHC measured by HTRF assay in Calu6 cells following treatment with indicated compounds. (E) Biochemical LONP1 IC_{50} (*y*-axis) and cell viability IC_{50} (*x*-axis) from LONP1-sensitive Calu6 and LONP1-insensitive H358 cell lines, respectively. Compounds are colored by their activity in the biochemical 20S proteasome assay. With the exception of bortezomib (red circle), only compounds with 20S proteasome IC_{50} > 10 μM (green) were tested in viability.

possibility exists that this density is a function of a five- and/or six-membered glycerol boronate formed from glycerol used in protein storage buffer and cryoprotection of crystals during harvesting, although we were unable to confirm it by mass spectrometry studies and is a subject of future studies.[35]

Changes in P2 Drive Selectivity by Reducing the 20S Proteasome Potency while Expansion into the Flexible P1 Pocket Drives Selectivity by Improving the LONP1 Potency. Despite the improved selectivity of **9a**, the potency toward the 20S proteasome was not entirely mitigated and a second round of SAR was initiated. Both the docking models and crystal structures suggested that further modification of the P3 pyrazine would be unlikely to lead to improved potency or selectivity due to the conserved backbone interaction points. We instead focused our efforts on both P1 and P2 substituents (Table 1). First, we explored the SAR at the P2 region by replacing the benzyl group with methyl (**9b**) or linear alkyls (**9c**–**e**). The activity on LONP1 was mostly unchanged (within ±2 fold). In contrast, there was a trend of loss of 20S potency with longer, unsubstituted alkyl chains (**9c**–**e**), probably due to the extension of these hydrophobic groups into a solvent-exposed region of the 20S proteasome. Interestingly, α-substituted groups [*e.g.*, *i*-Pr (**9f**) or *t*-Bu (**9g**)] trended toward reduced LONP1 potency, while replacing the benzyl group for a cyclohexylmethyl (**9h**) was tolerated on both proteases. Finally, removal of the chiral center with *gem*-dimethyl (**9i**) led to 14-fold reduction in potency compared to **9b**, suggesting the importance of the stereochemistry at P2.

The P1 binding region in both LONP1 and the 20S proteasome is fairly devoid of functional groups and both are relatively hydrophobic; however, in LONP1, the P1 binding site is more of a pocket, whereas in the 20S proteasome, it is more groove-like. Another notable difference is the relative size of the pockets. In the LONP1 crystal structures, the apo (PDB ID 6WYS) and bortezomib-bound (PDB ID 6X27) pockets are fairly similar in size, 212.7 and 223.7 $Å^3$, respectively. In the 20S proteasome, the apo pocket (PDB ID 5LE5) is 149.2 $Å^3$, slightly smaller than the pocket of LONP1; however, the bortezomib-bound pocket (PDB ID 5LF3) is more than double the size at 333.8 $Å^3$. Given the large difference between the apo and the bortezomib-bound pockets, we turned to molecular dynamics (MD) simulations to explore potential differences in binding site residue dynamics that could be exploited to improve compound selectivity (Figure 3A,B).

MD simulations of the protease domains of LONP1 and the 20S proteasome were performed both with and without bortezomib binding (PDBs: 6X27, 6WYS, 5LE3, and 5LF5). Interestingly, despite having a smaller pocket in the bortezomib-bound crystal form, the MD simulations suggest that, on average, the ligand binding pocket in LONP1 is not only larger but also more dynamic than that of the 20S proteasome (Figure 3A,B; Figure S2C,D). A detailed investigation of each binding site residue (Figure S3–S6) revealed that, in LONP1, residue L778 adopts several distinct,

https://doi.org/10.1021/acs.jmedchem.0c02152
J. Med. Chem. 2021, 64, 4857–4869

stable conformations that change the P1 pocket size and shape (Figures 3C and S3H). This is in contrast to the 20S proteasome where the back of the pocket is formed by a relatively invariable valine (V31, Figures S4−S6). This finding suggests that an increase in the size of the P1 substituent may be tolerated by LONP1 but less by the 20S proteasome.

To test this hypothesis, we synthesized a series of **9a** analogues with varying P1 substituents (Table 1, **11a−f**). Interestingly, replacing the isobutyl group of **9a** with larger substituents resulted in up to 10-fold improvements in LONP1 activity, yet no selectivity increases versus the 20S proteasome. Docking models extracted from the MD simulations of LONP1 suggested that P1 substituents up to 130 Å^3 (roughly the size of $(CH_2)_3Ph$) could be accommodated when L778 is in an upward facing conformation (Figure 3A,C). This finding was later confirmed by the co-structure of LONP1 with **12d** (PDB ID 6X1M), where the pocket volume expands from 212.7 to 292.7 Å^3, and L778 is found in an upward facing conformation (Figure 3C). Alternatively, in the 20S proteasome where the P1 pocket is less dynamic, large P1 substituents are predicted to fold up into the P1 groove, away from the center of the protein, while the P2 and P3 positions occupy roughly the same regions (Figure 3E). Based on these findings, we attribute the increase in potency on LONP1 to the flexibility of residue L778 and the sampling of a deep hydrophobic pocket that can be appropriately filled with large P1 groups (*e.g.*, **11d−e**).

In compounds with large P1 substituents, modification of the P2 position from aromatic to aliphatic was found to have a strong effect on the potency against the 20S proteasome. All compounds with a benzylic P2 substituent bind with at least moderate affinity to the 20S proteasome; however, when the P2 position is aliphatic, the binding drops off precipitously and is completely abolished when the P1 position is optimized (compounds **12a** and **d−g**). Despite the lack of observed binding affinity, the docking model does not provide a clear rationalization for this observation. As shown in Figure 3E, the model predicts that compounds with an aliphatic P2 substituent (**12a** and **d−g**) can be accommodated in a similar fashion as those with an aromatic P2 substituent (**9a**, **11a**, and **d−f**). Under the assumption that the docking model is accurate, this finding suggests that entropic factors rather than enthalpic contributions may be responsible for the loss in potency against the 20S proteasome.

Biochemically Potent LONP1 Inhibitors Demonstrate Potent Cellular Activity in LONP1-Dependent Cell Lines. Given the improved selectivity and potency profile of **12d**, we attempted to improve its overall physicochemical properties by modifying P3, a position that appeared less critical to overall binding based on docking. We prepared multiple analogues that included (hetero)aromatic or (hetero)-alkyl amides, carbamates, ureas, and sulfonamides as P3. All of them maintained sub-micromolar activity on LONP1, with only a fraction demonstrating 20S proteasome IC_{50} < 10 μM (Figure 4A), and all but one analogue having at least 80-fold selectivity versus the 20S proteasome. In an effort to differentiate these biochemically active and selective compounds, we turned our attention to cells to identify a pharmacodynamic (PD) biomarker that is altered upon inhibition of LONP1. Among all the analogues, **14** stood out as a potent and selective tool compound for *in vitro* LONP1 biology exploration. In fact, profiling of **14** in a protease panel at Nanosyn demonstrated its exquisite selectivity (Table S4). HEK293 cells stably expressing the LONP1-3X-FLAG construct were treated with **14** and subjected to an affinity purification and mass spectrometry analysis (Figure S7A). MMADHC was identified as an abundant protein PD biomarker that was significantly increased from treatment with **14** compared to dimethyl sulfoxide (DMSO) (Figure 4B). Although several other proteins were also enriched by **14** (Figure S7B−D), further confirmation of MMADHC induction by orthogonal methods was observed upon treatment of LONP1-dependent cell lines previously identified by genetic screens[36] (Figures 4C,D and S7E). Furthermore, **14** exhibited a ∼30−150-fold EC_{50} shift of MMADHC induction compared to bortezomib in Calu6, H1568, and H1944 (Figures 4D and S7E). Viability studies in both LONP1-dependent (Calu6) and independent (H358) lines further demonstrate the selectivity of **14** and analogues compared to bortezomib (Figure 4E). Thus, the biochemically potent LONP1 inhibitors result in a cellular increase of MMADHC and cell death in LONP1-dependent cell lines tested in this study.

CONCLUSIONS

In summary, we have described our efforts toward the identification of potent and selective boronic acid-based LONP1 inhibitors that can serve as tool compounds for the exploration of LONP1 biology. We have used X-ray crystallography and computational models to shed light on the LONP1 function and provide hypotheses on the structural differences of LONP1 and the 20S proteasome that led to the identification of selective LONP1 inhibitors. Studies aimed at understanding the impact of LONP1 upregulation in cancer are currently ongoing and data will be reported at due course.

Experimental Procedures. Unless otherwise noted, materials were obtained from commercial suppliers and were used without further purification. Removal of solvent under reduced pressure or concentration refers to distillation using Büchi or Heidolph rotary evaporators attached to a vacuum pump (3 mmHg). The products obtained as solids or high boiling oils were dried under vacuum (1 mmHg).

Purification of compounds by preparative RP-HPLC was achieved using a Waters autopurification system consisting of a 2767 autosampler/fraction collector, a 2545 binary gradient module, a 2489 UV detector, and a QDa mass spectrometer. The compounds were purified using a flow rate of 100 mL/min with a 50 mm × 19 mm i.d. Waters Atlantis T3 prep OBD 10 μm column (Waters, Milford, MA). A 3 min linear gradient from 10% solvent A [acetonitrile (MeCN) with 0.035% trifluoroacetic acid (TFA)] in solvent B (water [H_2O] with 0.05% TFA) to 30−90% A was used. Silica gel chromatography was performed by a CombiFlash (separation system R_f, TELEDYNE ISCO). Reverse-phase chromatography was performed by CombiFlash (separation system NEXTGEN 300+, TELEDYNE ISCO). ^{1}H NMR spectra were recorded on Avance-NEO with cryo-QNP (proton, carbon, phosphorous, and fluorine) (400 MHz) and Avance-III with smart probe (500 MHz) spectrometers. Proton resonances are reported in parts per million (ppm) downfield from tetramethylsilane (TMS). ^{1}H NMR data are reported as multiplicity (s, singlet; d, doublet; t, triplet; q, quartet; m, multiplets; dd, doublet of doublets; dt, doublet of triplets; dq, doublet of quartets; td, triplet of doublets; tt, triplet of triplets; ddd, doublet of doublet of doublets; and ddt, doublet of doublet of triplets). For spectra obtained in dimethylsulfoxide-d_6 (DMSO-d_6) and

https://doi.org/10.1021/acs.jmedchem.0c02152
J. Med. Chem. 2021, 64, 4857−4869

methanol-d_4 (CD_3OD), the residual protons (2.50 and 3.31 ppm, respectively) were used as the internal reference.

Purity of Compounds. The purity of all final compounds is ≥95%, as analyzed by an LC/MS system composed of an Agilent G1312B Binary Pump SL, an Agilent G1379B Degasser, an Agilent G1367C High-Performance Autosampler SL, an Agilent G1315C Diode Array Detector, a SOFT-A 1300 Evaporative Light Scattering Detector, and an Agilent G6140A MSD operated with ChemStation software. Samples were injected to the 0.9 mL per minute mobile phase flow starting at either 90% H_2O + 0.05% TFA (A) and 10% MeCN + 0.035% TFA (B) or 70% H_2O + 0.05% TFA (A) and 30% MeCN + 0.035% TFA (B), with a linear gradient to 90% B at 1.35 min, followed by 100% B from 1.36 to 1.95 min, and subsequent return to initial conditions until the end of the run at 2 min. The system employed a Waters Acquity HSS T3, 2.1 × 50.0 mm, 1.8 μ C18 column, which was kept at 60 °C. The mass spectrometer was operated in the positive mode with an electrospray voltage of 3 kV, nitrogen temperature at 350 °C, and skimmer set to 35 V. Chiral compounds were also analyzed by chiral HPLC or chiral SFC and demonstrated at least 95% ee.

General Procedure A: Amide Coupling. A mixture of carboxylic acid (1.1−1.3 equiv) and 1-[bis(dimethylamino)-methylene]-1*H*-1,2,3-triazolo[4,5-*b*]pyridinium 3-oxide hexafluorophosphate (HATU) or 2-(1*H*-benzo[*d*][1,2,3]triazol-1-yl)-1,1,3,3-tetramethyluronium (TBTU) (1.2−1.4 equiv) in dichloromethane (DCM) or dimethylformamide (DMF) (0.1−0.25 M) was cooled to −15 °C and then treated with diisopropylethylamine (DIEA) (3−4 equiv) and stirred for 5 min. The mixture was then treated with the corresponding amine (free base, hydrochloride, or trifluoroacetate) (1.0 equiv), stirred for 15 min at −15 °C, and then allowed to warm to room temperature. After 1−4 h, the reaction mixture was concentrated under reduced pressure and purified by reverse-phase chromatography (C_{18}, 30−100% MeCN/H_2O) to afford the desired amide.

General Procedure B: *tert*-Butyl Ester and *tert*-Butyl Carbamate Hydrolysis. The ester or carbamate (1.0 equiv) was treated with 4 M hydrochloric acid (HCl) in dioxane (20−50 equiv) and stirred for 16 h. The volatiles were removed under reduced pressure to afford the desired carboxylic acid or amine hydrochloride.

General Procedure C: Boronic Ester Hydrolysis. The amidoboronate was partitioned between heptane and 3 M HCl in MeOH (1:1 v/v, 15−30 equiv HCl) and then treated with isobutylboronic acid (10 equiv). The reaction mixture was stirred for 16 h, and then the layers were separated. The heptane layer was extracted once with MeOH and the combined MeOH extracts were washed twice with heptane. The MeOH solution was then concentrated under reduced pressure, partitioned between ethyl acetate (EtOAc) and saturated sodium bicarbonate ($NaHCO_3$), and the aqueous layer extracted twice with EtOAc. The combined organic layers were dried over sodium sulfate, concentrated under reduced pressure, and purified by reverse-phase chromatography (10−80% MeCN/H_2O) to afford the desired boronic acid.

*Synthesis of Compounds **3a−c**.* Compounds **3a−c** were prepared using general procedure A, followed by general procedure B. (*S*)-3-Phenyl-2-(pyrazine-2-carboxamido)-propanoic acid (**3a**, 2.06 g, 99%). ^{1}H NMR (500 MHz, DMSO-d_6): δ 13.04 (s, 1H), 9.14 (d, J = 1.5 Hz, 1H), 8.89 (d, J = 2.5 Hz, 1H), 8.86 (d, J = 8.2 Hz, 1H), 8.75 (dd, J = 2.5, 1.5 Hz, 1H), 7.28−7.21 (m, 4H), 7.18 (ddt, J = 6.6, 4.9, 2.7 Hz, 1H), 4.75 (td, J = 8.3, 5.3 Hz, 1H), 3.28−3.16 (m, 2H); ESMS m/z: 272.1 $(M + H)^+$.

(*R*)-3-Phenyl-2-(pyrazine-2-carboxamido)propanoic acid (**3b**, 2.06 g, 99% yield). ^{1}H NMR (400 MHz, DMSO-d_6): δ 9.13 (d, J = 1.5 Hz, 1H), 8.90−8.83 (m, 2H), 8.74 (dd, J = 2.5, 1.5 Hz, 1H), 7.22 (s, 4H), 7.21−7.13 (m, 1H), 4.74 (td, J = 8.2, 5.5 Hz, 1H), 3.26−3.15 (m, 2H); ESMS m/z: 272.1 $(M + H)^+$.

(*R*)-2-(Pyrazine-2-carboxamido)pentanoic acid (**3c**, 1.08 g, 100% yield). ESMS m/z: 224.2 $(M + H)^+$.

*Synthesis of Compounds **5a−b, 11a−f, 12a, and 12d−g**.* Compounds **5a−b**, **11a−f**, **12a**, and **12d−g** were prepared using general procedure A, followed by general procedure C. ((*S*)-3-Methyl-1-((*S*)-3-phenyl-2-(pyrazine-2-carboxamido)-propanamido)butyl)boronic acid (**5a**, 4 mg, 10%). ^{1}H NMR (400 MHz, methanol-d_4): δ 9.18 (dd, J = 8.4, 1.5 Hz, 1H), 8.80 (dd, J = 5.2, 2.5 Hz, 1H), 8.70 (ddd, J = 4.2, 2.5, 1.6 Hz, 1H), 7.34−7.26 (m, 4H), 7.26−7.19 (m, 1H), 5.15−5.00 (m, 1H), 3.28−3.19 (m, 2H), 2.69 (t, J = 7.7 Hz, 1H), 1.63−1.31 (m, 2H), 1.22−1.19 (m, 1H), 0.87 (ddd, J = 14.3, 6.6, 5.0 Hz, 6H); ESMS m/z: 407.2 $(M + Na)^+$.

((*S*)-3-Methyl-1-((*R*)-3-phenyl-2-(pyrazine-2-carboxamido)propanamido)butyl)boronic acid (**5b**, 3 mg, 73% yield). ^{1}H NMR (400 MHz, methanol-d_4): δ 9.17 (dd, J = 1.5, 8.4 Hz, 1H), 8.80 (dd, J = 2.5, 5.1 Hz, 1H), 8.70 (ddd, J = 1.5, 2.5, 4.3 Hz, 1H), 7.33−7.27 (m, 4H), 7.27−7.21 (m, 1H), 5.17−5.00 (m, 1H), 3.25−3.20 (m, 2H), 2.69 (t, J = 7.7 Hz, 1H), 1.65−1.30 (m, 2H), 1.29−0.98 (m, 1H), 0.85 (dd, J = 6.6, 4.8 Hz, 6H); ESMS m/z: 407.2 $(M + Na)^+$.

((*R*)-2-Cyclohexyl-1-((*R*)-3-phenyl-2-(pyrazine-2-carboxamido)propanamido)ethyl)boronic acid (**11a**, 11 mg, 84% yield). ^{1}H NMR (400 MHz, methanol-d_4): δ 9.18 (dd, J = 1.5, 8.8 Hz, 1H), 8.80 (dd, J = 2.5, 5.1 Hz, 1H), 8.71 (ddd, J = 1.5, 2.5, 4.2 Hz, 1H), 7.34−7.27 (m, 4H), 7.27−7.18 (m, 1H), 5.19−4.99 (m, 1H), 3.28−3.24 (m, 1H), 2.72 (dd, J = 5.9, 9.2 Hz, 1H), 1.80 (d, J = 13.1 Hz, 1H), 1.73−1.55 (m, 4H), 1.39−1.27 (m, 2H), 1.27−1.01 (m, 5H), 0.93−0.75 (m, 2H); ESMS m/z: 407.3 $(M - H_2O + H)^+$.

((*R*)-5-Methyl-1-((*R*)-3-phenyl-2-(pyrazine-2-carboxamido)propanamido)hexyl)boronic acid (**11b**, 8 mg, 59% yield). ^{1}H NMR (400 MHz, methanol-d_4): δ 9.17 (dd, J = 1.5, 7.0 Hz, 1H), 8.80 (dd, J = 2.5, 4.1 Hz, 1H), 8.70 (ddd, J = 1.5, 2.5, 3.3 Hz, 1H), 7.34−7.25 (m, 4H), 7.25−7.18 (m, 1H), 5.15−4.99 (m, 1H), 3.26−3.22 (m, 1H), 2.56 (t, J = 6.9 Hz, 1H), 1.59−1.48 (m, 1H), 1.48−1.27 (m, 3H), 1.27−1.09 (m, 4H), 0.89−0.85 (m, 6H); ESMS m/z: 395.3 $(M - H_2O + H)^+$.

((*R*)-6-Bromo-1-((*R*)-3-phenyl-2-(pyrazine-2-carboxamido)propanamido)hexyl)boronic acid (**11c**, 21 mg, 69% yield). ^{1}H NMR (400 MHz, methanol-d_4): δ 9.19 (d, J = 1.5 Hz, 1H), 8.79 (d, J = 2.5 Hz, 1H), 8.68 (dd, J = 2.5, 1.5 Hz, 1H), 7.28−7.24 (m, 4H), 7.23−7.17 (m, 1H), 4.84−4.77 (m, 1H), 3.42 (t, J = 6.8 Hz, 2H), 3.17 (dd, J = 6.6, 1.8 Hz, 1H), 3.15−3.07 (m, 2H), 1.87−1.77 (m, 2H), 1.47−1.38 (m, 4H), 1.29−1.19 (m, 2H); ESMS m/z: 459.1 $(M - H_2O + H)^+$.

((*R*)-4-Phenyl-1-((*R*)-3-phenyl-2-(pyrazine-2-carboxamido)propanamido)butyl)boronic acid (**11d**, 8 mg, 53% yield). ^{1}H NMR (400 MHz, methanol-d_4): δ 9.17 (dd, J = 1.5, 9.0 Hz, 1H), 8.80 (dd, J = 2.5, 4.7 Hz, 1H), 8.70 (ddd, J = 1.5, 2.5, 4.2 Hz, 1H), 7.32−7.27 (m, 3H), 7.27−7.20 (m, 4H), 7.17−7.09 (m, 3H), 5.12−5.01 (m, 1H), 3.37−3.34 (m, 1H), 3.26−3.17 (m, 1H), 2.65−2.49 (m, 3H), 1.69−1.57 (m, 1H),

https://doi.org/10.1021/acs.jmedchem.0c02152
J. Med. Chem. 2021, 64, 4857−4869

1.49 (ddt, J = 7.3, 14.6, 29.7 Hz, 2H), 1.35−1.23 (m, 1H); ESMS m/z: 429.3 $(M - H_2O + H)^+$.

((*R*)-3-Phenyl-1-((*R*)-3-phenyl-2-(pyrazine-2-carboxamido)propanamido)propyl)boronic acid (**11e**, 9 mg, 93% yield). ^{1}H NMR (400 MHz, methanol-d_4): δ 9.18 (s, 1H), 8.80 (s, 1H), 8.70 (s, 1H), 7.34−7.27 (m, 4H), 7.25−7.19 (m, 3H), 7.18−7.08 (m, 3H), 5.14−5.03 (m, 1H), 3.28−3.21 (m, 2H), 2.61 (q, J = 7.1, 8.4 Hz, 2H), 2.50 (t, J = 7.1 Hz, 1H), 1.88−1.71 (m, 1H), 1.70−1.46 (m, 1H); ESMS m/z: 415.2 $(M - H_2O + H)^+$.

((*R*)-2-Phenyl-1-((*R*)-3-phenyl-2-(pyrazine-2-carboxamido)propanamido)ethyl)boronic acid (**11f**, 9 mg, 86% yield). ^{1}H NMR (400 MHz, methanol-d_4): δ 9.17 (d, J = 6.5 Hz, 1H), 8.87−8.72 (m, 1H), 8.69 (d, J = 2.2 Hz, 1H), 7.38−7.23 (m, 5H), 7.23−7.15 (m, 3H), 7.15−7.07 (m, 1H), 7.03−6.97 (m, 1H), 5.12−4.98 (m, 1H), 3.27−3.16 (m, 2H), 2.93−2.73 (m, 2H), 2.68−2.30 (m, 1H); ESMS m/z: 401.20 $(M - H_2O + H)^+$.

((*R*)-2-Cyclohexyl-1-((*R*)-2-(pyrazine-2-carboxamido)-pentanamido)ethyl)boronic acid (**12a**, 9 mg, 45% yield). ^{1}H NMR (400 MHz, methanol-d_4): δ 9.24 (d, J = 1.4 Hz, 1H), 8.82 (d, J = 2.5 Hz, 1H), 8.73 (dd, J = 2.5, 1.5 Hz, 1H), 4.87−4.80 (m, 1H), 2.76 (t, J = 6.9 Hz, 1H), 1.98−1.85 (m, 2H), 1.76−1.66 (m, 4H), 1.59−1.40 (m, 3H), 1.40−1.31 (m, 3H), 1.30−1.17 (m, 3H), 1.00 (t, J = 7.4 Hz, 3H), 0.97−0.77 (m, 2H); ESMS m/z: 359.3 $(M - H_2O + H)^+$.

((*R*)-4-Phenyl-1-((*R*)-2-(pyrazine-2-carboxamido)-pentanamido)butyl)boronic acid (**12d**, 15 mg, 84% yield). ^{1}H NMR (400 MHz, methanol-d_4): δ 9.23 (d, J = 1.5 Hz, 1H), 8.82 (d, J = 2.5 Hz, 1H), 8.72 (dd, J = 2.5, 1.5 Hz, 1H), 7.25−7.19 (m, 2H), 7.19−7.15 (m, 2H), 7.14−7.09 (m, 1H), 4.83 (dd, J = 8.9, 5.7 Hz, 1H), 2.69−2.53 (m, 3H), 2.04−1.80 (m, 2H), 1.80−1.61 (m, 2H), 1.61−1.34 (m, 4H), 0.99 (t, J = 7.4 Hz, 3H); ESMS m/z: 381.3 $(M - H_2O + H)^+$.

((*R*)-3-Phenyl-1-((*R*)-2-(pyrazine-2-carboxamido)-pentanamido)propyl)boronic acid (**12e**, 29 mg, 62% yield). ^{1}H NMR (500 MHz, methanol-d_4): δ 9.14 (d, J = 1.5 Hz, 1H), 8.70 (d, J = 2.5 Hz, 1H), 8.64−8.58 (m, 1H), 7.17−7.05 (m, 4H), 7.02 (td, J = 7.0, 3.3 Hz, 1H), 4.77−4.74 (m, 1H), 2.62−2.48 (m, 3H), 1.93−1.79 (m, 2H), 1.74 (ddt, J = 13.3, 9.7, 6.6 Hz, 1H), 1.63 (ddt, J = 13.7, 9.4, 6.6 Hz, 1H), 1.38 (m, 2H), 0.89 (t, J = 7.4 Hz, 3H); ESMS m/z: 367.2 $(M - H_2O + H)^+$.

((*R*)-2-Phenyl-1-((*R*)-2-(pyrazine-2-carboxamido)-pentanamido)ethyl)boronic acid (**12f**, 24 mg, 45% yield). ^{1}H NMR (500 MHz, methanol-d_4): δ 9.13 (dd, J = 1.5, 6.9 Hz, 1H), 8.71 (dd, J = 2.5, 4.9 Hz, 1H), 8.60 (ddd, J = 1.5, 2.5, 6.6 Hz, 1H), 7.14 (d, J = 4.8 Hz, 1H), 7.11−6.98 (m, 4H), 4.71−4.64 (m, 1H), 2.88−2.74 (m, 2H), 2.52 (td, J = 9.3, 14.2 Hz, 1H), 1.87−1.72 (m, 2H), 1.46−1.26 (m, 2H), 0.93−0.83 (m, 3H); ESMS m/z: 353.2 $(M - H_2O + H)^+$.

((*R*)-1-((*R*)-2-(Pyrazine-2-carboxamido)pentanamido)-pentyl)boronic acid (**12g**, 19 mg, 36% yield). ^{1}H NMR (400 MHz, methanol-d_4): δ 9.24 (d, J = 1.5 Hz, 1H), 8.82 (d, J = 2.5 Hz, 1H), 8.73 (dd, J = 1.5, 2.5 Hz, 1H), 4.88−4.81 (m, 1H), 2.59 (t, J = 7.3 Hz, 1H), 2.04−1.86 (m, 2H), 1.59−1.28 (m, 8H), 1.00 (t, J = 7.4 Hz, 3H), 0.96−0.87 (m, 3H); ESMS m/z: 319.2 $(M - H_2O + H)^+$.

Synthesis of Compounds ***8a−i, 13.*** Compounds **8a−i**, **13** were prepared using general procedure A. *tert*-Butyl((*R*)-1-(((*R*)-3-methyl-1-((3a*S*,4*S*,6*S*,7a*R*)-3a,5,5-trimethylhexahydro-4,6-methanobenzo[*d*][1,3,2]dioxaborol-2-yl)butyl)amino)-1-oxo-3-phenylpropan-2-yl)carbamate (**8a**, 64 mg, 95%). ^{1}H NMR (400 MHz, methanol-d_4): δ 7.26 (m, 5H), 4.51 (dd, J = 8.5, 6.3 Hz, 1H), 4.21 (dd, J = 8.6, 2.2 Hz, 1H), 3.13 (dd, J = 13.7, 6.0 Hz, 1H), 2.87 (dd, J = 13.7, 8.8 Hz, 1H), 2.65 (t, J = 7.7 Hz, 1H), 2.41−2.29 (m, 1H), 2.14 (ddd, J = 10.0, 6.0, 1.8 Hz, 1H), 1.98 (t, J = 5.5 Hz, 1H), 1.88 (tt, J = 5.6, 2.9 Hz, 1H), 1.81 (dt, J = 14.1, 2.5 Hz, 1H), 1.71 (dt, J = 13.4, 6.7 Hz, 1H), 1.48 (d, J = 10.3 Hz, 1H), 1.41 (s, 3H), 1.33 (m, 12H), 0.96−0.83 (s, 9H); ESMS m/z: 513.4 $(M + H)^+$.

tert-Butyl((*R*)-1-(((*R*)-3-methyl-1-((3a*S*,4*S*,6*S*,7a*R*)-3a,5,5-trimethylhexahydro-4,6-methanobenzo[*d*][1,3,2]dioxaborol-2-yl)butyl)amino)-1-oxopropan-2-yl)carbamate (**8b**, 118 mg, 69% yield). ^{1}H NMR (400 MHz, methanol-d_4): δ 4.40−4.24 (m, 1H), 4.18 (dd, J = 8.8, 2.3 Hz, 1H), 2.70 (t, J = 7.7 Hz, 1H), 2.43−2.27 (m, 1H), 2.22−2.07 (m, 1H), 1.95 (t, J = 5.6 Hz, 1H), 1.86 (td, J = 5.7, 2.9 Hz, 1H), 1.80 (d, J = 6.0 Hz, 1H), 1.76 (d, J = 5.8 Hz, 1H), 1.49−1.46 (m, 1H), 1.45 (s, 9H), 1.41 (s, 1H), 1.39 (s, 1H), 1.37 (s, 3H), 1.35 (d, J = 7.2 Hz, 3H), 1.29 (s, 3H), 0.93 (dd, J = 6.6, 1.9 Hz, 6H), 0.88 (s, 3H); ESMS m/z: 437.4 $(M + H)^+$.

tert-Butyl((*R*)-1-(((*R*)-3-methyl-1-((3a*S*,4*S*,6*S*,7a*R*)-3a,5,5-trimethylhexahydro-4,6-methanobenzo[*d*][1,3,2]dioxaborol-2-yl)butyl)amino)-1-oxobutan-2-yl)carbamate (**8c**, 131 mg, 75% yield). ^{1}H NMR (400 MHz, methanol-d_4): δ 4.28−4.09 (m, 2H), 2.69 (t, J = 7.8 Hz, 1H), 2.33 (ddt, J = 11.1, 8.9, 2.5 Hz, 1H), 2.19−2.06 (m, 1H), 1.95 (t, J = 5.6 Hz, 1H), 1.86 (dq, J = 5.6, 2.8 Hz, 1H), 1.82 (d, J = 12.4 Hz, 1H), 1.79 (d, J = 3.5 Hz, 1H), 1.77 (d, J = 3.2 Hz, 1H), 1.75 (d, J = 6.9 Hz, 1H), 1.66 (dt, J = 14.4, 7.6 Hz, 1H), 1.45 (s, 9H), 1.40−1.38 (m, 1H), 1.37 (s, 3H), 1.36−1.34 (m, 1H), 1.29 (s, 3H), 0.97 (t, J = 7.4 Hz, 3H), 0.93 (d, J = 6.6 Hz, 6H), 0.88 (s, 3H); ESMS m/z: 451.4 $(M + H)^+$.

tert-Butyl((*R*)-1-(((*R*)-3-methyl-1-((3a*S*,4*S*,6*S*,7a*R*)-3a,5,5-trimethylhexahydro-4,6-methanobenzo[*d*][1,3,2]dioxaborol-2-yl)butyl)amino)-1-oxopentan-2-yl)carbamate (**8d**, 125 mg, 70% yield). ^{1}H NMR (400 MHz, methanol-d_4): δ 4.25 (dd, J = 9.0, 5.7 Hz, 1H), 4.17 (dd, J = 8.8, 2.3 Hz, 1H), 2.72−2.66 (m, 1H), 2.40−2.29 (m, 1H), 2.17−2.08 (m, 1H), 1.95 (t, J = 5.6 Hz, 1H), 1.90−1.82 (m, 1H), 1.81−1.78 (m, 1H), 1.78−1.76 (m, 1H), 1.76−1.71 (m, 1H), 1.71−1.64 (m, 1H), 1.64−1.57 (m, 1H), 1.48 (s, 1H), 1.45 (s, 9H), 1.42−1.38 (m, 2H), 1.37 (s, 3H), 1.36−1.33 (m, 1H), 1.29 (s, 3H), 0.96 (t, J = 7.4 Hz, 3H), 0.93 (d, J = 6.2 Hz, 6H), 0.88 (s, 3H); ESMS m/z: 465.4 $(M + H)^+$.

tert-Butyl((*R*)-1-(((*R*)-3-methyl-1-((3a*S*,4*S*,6*S*,7a*R*)-3a,5,5-trimethylhexahydro-4,6-methanobenzo[*d*][1,3,2]dioxaborol-2-yl)butyl)amino)-1-oxohexan-2-yl)carbamate (**8e**, 86 mg, 46% yield). ^{1}H NMR (400 MHz, methanol-d_4): δ 4.23 (t, J = 7.4 Hz, 1H), 4.17 (dd, J = 8.7, 2.3 Hz, 1H), 2.68 (t, J = 7.7 Hz, 1H), 2.42−2.28 (m, 1H), 2.18−2.05 (m, 1H), 1.95 (t, J = 5.6 Hz, 1H), 1.89−1.83 (m, 1H), 1.82−1.78 (m, 1H), 1.78−1.70 (m, 2H), 1.69−1.56 (m, 1H), 1.48 (s, 1H), 1.45 (s, 9H), 1.38 (s, 2H), 1.37 (s, 3H), 1.36 (s, 4H), 1.29 (s, 3H), 0.96−0.89 (m, 9H), 0.88 (s, 3H); ESMS m/z: 479.4 $(M + H)^+$.

tert-Butyl((*R*)-3-methyl-1-(((*R*)-3-methyl-1-((3a*S*,4*S*,6*S*,7a*R*)-3a,5,5-trimethylhexahydro-4,6-methanobenzo[*d*][1,3,2]dioxaborol-2-yl)butyl)amino)-1-oxobutan-2-yl)carbamate (**8f**, 118 mg, 66% yield). ^{1}H NMR (400 MHz, methanol-d_4): δ 4.17 (dd, J = 8.8, 2.3 Hz, 1H), 4.07 (d, J = 7.2 Hz, 1H), 2.68 (t, J = 7.7 Hz, 1H), 2.34 (ddd, J = 14.2, 6.9, 4.5 Hz, 1H), 2.18−2.09 (m, 1H), 2.09−2.00 (m, 1H), 1.96 (t, J = 5.6 Hz, 1H), 1.86 (tt, J = 5.6, 3.0 Hz, 1H), 1.82−1.78 (m, 1H), 1.78−1.70 (m, 1H), 1.47 (s, 1H), 1.45 (s, 9H), 1.38 (s, 1H), 1.37 (s, 3H), 1.35 (s, 1H), 1.29 (s, 3H), 0.96 (s, 3H), 0.95−

https://doi.org/10.1021/acs.jmedchem.0c02152
J. Med. Chem. 2021, 64, 4857−4869

0.93 (m, 6H), 0.92 (s, 3H), 0.88 (s, 3H); ESMS *m/z*: 465.4 $(M + H)^+$.

tert-Butyl((*R*)-3,3-dimethyl-1-(((*R*)-3-methyl-1-((3a*S*,4*S*,6-*S*,7a*R*)-3a,5,5-trimethylhexahydro-4,6-methanobenzo[*d*]-[1,3,2]dioxaborol-2-yl)butyl)amino)-1-oxobutan-2-yl)-carbamate (**8g**, 112 mg, 61% yield). ^{1}H NMR (400 MHz, methanol-d_4): δ 4.22−4.06 (m, 2H), 2.65 (t, *J* = 7.7 Hz, 1H), 2.40−2.27 (m, 1H), 2.20−2.07 (m, 1H), 1.96 (t, *J* = 5.6 Hz, 1H), 1.86 (tt, *J* = 5.6, 3.0 Hz, 1H), 1.82−1.70 (m, 2H), 1.50−1.46 (m, 1H), 1.45 (s, 9H), 1.38 (s, 3H), 1.37−1.33 (m, 2H), 1.29 (s, 3H), 1.00 (s, 9H), 0.93 (d, *J* = 6.8 Hz, 6H), 0.88 (s, 3H); ESMS *m/z*: 479.4 $(M + H)^+$.

tert-Butyl((*R*)-3-cyclohexyl-1-(((*R*)-3-methyl-1-((3a*S*,4*S*,6-*S*,7a*R*)-3a,5,5-trimethylhexahydro-4,6-methanobenzo[*d*]-[1,3,2]dioxaborol-2-yl)butyl)amino)-1-oxopropan-2-yl)-carbamate (**8h**, 97 mg, 48% yield). ^{1}H NMR (400 MHz, methanol-d_4): δ 4.36 (dd, *J* = 9.9, 5.5 Hz, 1H), 4.17 (dd, *J* = 8.8, 2.3 Hz, 1H), 2.67 (t, *J* = 7.7 Hz, 1H), 2.42−2.26 (m, 1H), 2.21−2.06 (m, 1H), 1.95 (t, *J* = 5.6 Hz, 1H), 1.90−1.83 (m, 1H), 1.83−1.75 (m, 3H), 1.72 (d, *J* = 13.5 Hz, 3H), 1.65 (s, 1H), 1.62−1.57 (m, 1H), 1.54 (dd, *J* = 9.6, 5.2 Hz, 1H), 1.48 (s, 1H), 1.45 (s, 9H), 1.41 (s, 2H), 1.37 (s, 3H), 1.35−1.30 (m, 2H), 1.29 (s, 3H), 1.27−1.23 (m, 1H), 1.23−1.12 (m, 2H), 1.05−0.96 (m, 1H), 0.93 (d, *J* = 6.5 Hz, 6H), 0.88 (m, 3H); ESMS *m/z*: 519.5 $(M + H)^+$.

2,4-Dimethyl-*N*-((*R*)-1-oxo-1-(((*R*)-4-phenyl-1-((3a*S*,4*S*,6-*S*,7a*R*)-3a,5,5-trimethylhexahydro-4,6-methanobenzo[*d*]-[1,3,2]dioxaborol-2-yl)butyl)amino)pentan-2-yl)oxazole-5-carboxamide (**13**, 27.7 g, 77% yield). ^{1}H NMR (400 MHz, methanol-d_4): δ 7.25−7.19 (m, 2H), 7.19−7.14 (m, 2H), 7.15−7.09 (m, 1H), 4.72 (dd, *J* = 9.4, 5.7 Hz, 1H), 4.17 (dd, *J* = 8.8, 2.3 Hz, 1H), 2.71−2.55 (m, 3H), 2.50 (s, 3H), 2.39 (s, 3H), 2.37−2.28 (m, 1H), 2.16−2.06 (m, 1H), 1.95 (t, *J* = 5.6 Hz, 1H), 1.91−1.81 (m, 2H), 1.81−1.69 (m, 4H), 1.65−1.53 (m, 1H), 1.53−1.48 (m, 1H), 1.48−1.38 (m, 3H), 1.37 (s, 3H), 1.29 (s, 3H), 0.97 (t, *J* = 7.4 Hz, 3H), 0.88 (s, 3H); ESMS *m/z*: 550.4 $(M + H)^+$.

*Synthesis of Compounds **9a−i**, **14**.* Compounds **9a−i**, **14** were prepared using general procedure B, followed by general procedure A, followed by general procedure C. ((*R*)-3-Methyl-1-((*R*)-3-phenyl-2-(pyrazine-2-carboxamido)propanamido)-butyl)boronic acid (**9a**, 17 mg, 44% yield). ^{1}H NMR (400 MHz, methanol-d_4): δ 9.16 (d, *J* = 1.5 Hz, 1H), 8.79 (d, *J* = 2.5 Hz, 1H), 8.69 (dd, *J* = 2.5, 1.5 Hz, 1H), 7.35−7.17 (m, 5H), 5.15−5.04 (m, 1H), 3.35 (s, 1H), 3.22 (dd, *J* = 13.8, 8.4 Hz, 1H), 2.68 (t, *J* = 7.6 Hz, 1H), 1.59 (dq, *J* = 13.2, 6.7 Hz, 1H), 1.33 (t, *J* = 7.4 Hz, 2H), 0.88 (dd, *J* = 6.6, 4.9 Hz, 6H); ESMS *m/z*: 367.2 $(M - H_2O + H)^+$.

((*R*)-3-Methyl-1-((*R*)-2-(pyrazine-2-carboxamido)-propanamido)butyl)boronic acid (**9b**, 17 mg, 66% yield). ^{1}H NMR (400 MHz, methanol-d_4): δ 9.23 (d, *J* = 1.5 Hz, 1H), 8.80 (d, *J* = 2.5 Hz, 1H), 8.73−8.69 (m, 1H), 4.89 (q, *J* = 7.2 Hz, 1H), 2.73 (t, *J* = 7.6 Hz, 1H), 1.70−1.65 (m, 1H), 1.58 (d, *J* = 7.2 Hz, 3H), 1.36 (t, *J* = 7.3 Hz, 2H), 0.92 (d, *J* = 2.4 Hz, 3H), 0.90 (d, *J* = 2.4 Hz, 3H); ESMS *m/z*: 291.3 $(M - H_2O + H)^+$.

((*R*)-3-Methyl-1-((*R*)-2-(pyrazine-2-carboxamido)-butanamido)butyl)boronic acid (**9c**, 17 mg, 79% yield). ^{1}H NMR (400 MHz, methanol-d_4): δ 9.24 (d, *J* = 1.5 Hz, 1H), 8.81 (d, *J* = 2.5 Hz, 1H), 8.72 (dd, *J* = 2.5, 1.5 Hz, 1H), 4.74 (dd, *J* = 8.6, 5.9 Hz, 1H), 2.74 (t, *J* = 7.6 Hz, 1H), 2.14−1.99 (m, 1H), 1.99−1.86 (m, 1H), 1.78−1.59 (m, 1H), 1.36 (t, *J* = 7.3 Hz, 2H), 1.05 (t, *J* = 7.4 Hz, 3H), 0.92 (d, *J* = 2.2 Hz, 3H), 0.91 (d, *J* = 2.1 Hz, 3H); ESMS *m/z*: 305.3 $(M - H_2O + H)^+$.

((*R*)-3-Methyl-1-((*R*)-2-(pyrazine-2-carboxamido)-pentanamido)butyl)boronic acid (**9d**, 19 mg, 67% yield). ^{1}H NMR (400 MHz, methanol-d_4): δ 9.24 (d, *J* = 1.5 Hz, 1H), 8.81 (d, *J* = 2.5 Hz, 1H), 8.72 (dd, *J* = 2.5, 1.5 Hz, 1H), 4.88−4.84 (m, 1H), 2.73 (t, *J* = 7.6 Hz, 1H), 2.03−1.83 (m, 2H), 1.74−1.61 (m, 1H), 1.59−1.38 (m, 2H), 1.35 (t, *J* = 7.3 Hz, 2H), 0.99 (t, *J* = 7.4 Hz, 3H), 0.92 (d, *J* = 2.2 Hz, 3H), 0.90 (d, *J* = 2.3 Hz, 3H); ESMS *m/z*: 319.3 $(M - H_2O + H)^+$.

((*R*)-3-Methyl-1-((*R*)-2-(pyrazine-2-carboxamido)-hexanamido)butyl)boronic acid (**9e**, 20 mg, 71% yield). ^{1}H NMR (400 MHz, methanol-d_4): δ 9.24 (d, *J* = 1.5 Hz, 1H), 8.81 (d, *J* = 2.5 Hz, 1H), 8.72 (dd, *J* = 2.5, 1.5 Hz, 1H), 4.81−4.79 (m, 1H), 2.73 (t, *J* = 7.6 Hz, 1H), 2.10−1.95 (m, 1H), 1.95−1.82 (m, 1H), 1.74−1.58 (m, 1H), 1.54−1.37 (m, 4H), 1.35 (t, *J* = 7.3 Hz, 2H), 0.99−0.92 (m, 3H), 0.92 (d, *J* = 2.1 Hz, 3H), 0.91 (d, *J* = 2.1 Hz, 3H); ESMS *m/z*: 333.3 $(M - H_2O + H)^+$.

((*R*)-3-Methyl-1-((*R*)-3-methyl-2-(pyrazine-2-carboxamido)butanamido)butyl)boronic acid (**9f**, 24 mg, 78% yield). ^{1}H NMR (400 MHz, methanol-d_4): δ 9.24 (d, *J* = 1.5 Hz, 1H), 8.82 (d, *J* = 2.5 Hz, 1H), 8.72 (dd, *J* = 2.5, 1.5 Hz, 1H), 4.64 (d, *J* = 7.6 Hz, 1H), 2.75 (t, *J* = 7.6 Hz, 1H), 2.43−2.22 (m, 1H), 1.79−1.58 (m, 1H), 1.42−1.29 (m, 2H), 1.06 (t, *J* = 6.4 Hz, 6H), 0.93 (d, *J* = 1.7 Hz, 3H), 0.91 (d, *J* = 1.7 Hz, 3H); ESMS *m/z*: 319.3 $(M - H_2O + H)^+$.

((*R*)-1-((*R*)-3,3-Dimethyl-2-(pyrazine-2-carboxamido)-butanamido)-3-methylbutyl)boronic acid (**9g**, 24 mg, 77% yield). ^{1}H NMR (400 MHz, methanol-d_4): δ 9.26 (d, *J* = 1.5 Hz, 1H), 8.84 (d, *J* = 2.5 Hz, 1H), 8.72 (dd, *J* = 2.5, 1.5 Hz, 1H), 4.73 (s, 1H), 2.74 (t, *J* = 7.6 Hz, 1H), 1.77−1.60 (m, 1H), 1.38−1.32 (m, 2H), 1.12 (s, 9H), 0.93 (d, *J* = 2.1 Hz, 3H), 0.92 (d, *J* = 2.2 Hz, 3H); ESMS *m/z*: 333.3 $(M - H_2O + H)^+$.

((*R*)-1-((*R*)-3-Cyclohexyl-2-(pyrazine-2-carboxamido)-propanamido)-3-methylbutyl)boronic acid (**9h**, 28 mg, 72% yield). ^{1}H NMR (400 MHz, methanol-d_4): δ 9.24 (d, *J* = 1.5 Hz, 1H), 8.81 (d, *J* = 2.5 Hz, 1H), 8.72 (dd, *J* = 2.5, 1.5 Hz, 1H), 4.94 (dd, *J* = 9.8, 5.5 Hz, 1H), 2.71 (t, *J* = 7.6 Hz, 1H), 1.87−1.78 (m, 3H), 1.74 (ddd, *J* = 15.3, 5.9, 3.7 Hz, 3H), 1.69−1.59 (m, 2H), 1.49−1.38 (m, 1H), 1.34 (t, *J* = 7.3 Hz, 2H), 1.30−1.24 (m, 1H), 1.20 (dd, *J* = 11.3, 8.3 Hz, 2H), 1.10−0.94 (m, 2H), 0.92 (d, *J* = 2.0 Hz, 3H), 0.90 (d, *J* = 2.0 Hz, 3H); ESMS *m/z*: 373.3 $(M - H_2O + H)^+$.

(*R*)-(3-Methyl-1-(2-methyl-2-(pyrazine-2-carboxamido)-propanamido)butyl)boronic acid (**9i**, 10 mg, 17% yield). ^{1}H NMR (400 MHz, methanol-d_4): δ 9.20 (d, *J* = 1.5 Hz, 1H), 8.81 (d, *J* = 2.6 Hz, 1H), 8.71 (dd, *J* = 2.5, 1.5 Hz, 1H), 2.71 (t, *J* = 7.6 Hz, 1H), 1.69 (s, 7H), 1.42−1.30 (m, 2H), 0.90 (dd, *J* = 6.6, 0.9 Hz, 6H); ESMS *m/z*: 305.2 $(M - H_2O + H)^+$.

((*R*)-1-((*R*)-2-(2,4-Dimethyloxazole-5-carboxamido)-pentanamido)-4-phenylbutyl)boronic acid (**14**, 30 mg, 72% yield). ^{1}H NMR (400 MHz, methanol-d_4): δ 7.27−7.20 (m, 2H), 7.20−7.16 (m, 2H), 7.15−7.10 (m, 1H), 4.73 (dd, *J* = 5.7, 9.3 Hz, 1H), 2.71−2.51 (m, 3H), 2.50 (s, 3H), 2.38 (s, 3H), 1.96−1.78 (m, 2H), 1.70 (m, 2H), 1.59−1.37 (m, 4H), 0.98 (t, *J* = 7.4 Hz, 3H); ESMS *m/z*: 398.3 $(M - H_2O + H)^+$.

Biochemical LONP1 Protease Assay. The biochemical LONP1 protease assay was carried out in a 384-well format utilizing the 5-FAM (fluorophore) and QXL520 (quencher) pair. The final assay mixture contains 10 mM Tris pH 7.5, 50 mM NaCl, 10 mM $CaCl_2$, 2 mM DTT, 0.01% BSA, 40 nM

https://doi.org/10.1021/acs.jmedchem.0c02152
J. Med. Chem. 2021, 64, 4857−4869

LONP1, 1 μM ATP, and 10 μM of fluorogenic peptide substrate QXL520-YRGITCSGRQK(5-FAM)-NH_2 in a total volume of 10 μL. The assay was carried out at room temperature for 50 min, and fluorescence was read on a PheraStar reader. As the quencher and fluorophore are built into the peptide, no change in fluorescence will be detected unless the peptide is cleaved by the enzyme.

LONP1 HTS. The biochemical LONP1 protease assay was further miniaturized into a 1536-well format for HTS. The assay condition remained similar with a reduction in reaction volume (6 μL) and enzyme concentration (25 nM). The final compound concentration in the screen was either 10 μM or 50 μM (depending on the stock concentration). The HTS was performed on a GNF automation system.

Biochemical 20S Protease Assay. The biochemical 20S protease assay was carried out in the same format as the LONP1 protease assay. The final assay mixture contains 10 mM Tris pH 7.5, 50 mM NaCl, 2 mM DTT, 0.01% BSA, 0.025% SDS, 0.571 nM 20S proteasome (ENZO, Cat # BML-PW8720-0050), and 10 μM of fluorogenic peptide substrate QXL520-YRGITCSGRQK(5-FAM)-NH_2 in a total volume of 10 μL. The enzyme solution (in reaction buffer) was first incubated at room temperature for 10 min to allow the 20S activation by SDS, followed by addition of substrate peptide to start the reaction. The assay was carried out at room temperature for 60 min, and fluorescence was read on a PheraStar reader.

IC_{50} Determination. Compounds were serial-diluted and Echo-transferred (50 nL) into the reaction plate. The compound and enzyme mixture was first incubated at room temperature for 15 min, and then the substrate mixture was added to start the reaction. The final compound concentrations ranged from 0.00028 to 50 μM, and IC_{50} values were determined from the resulting 12-point inhibition curves based on the Michaelis–Menten equation.

Cellular Assays. All cell lines were purchased from ATCC and maintained as described previously.[37] One thousand cells were seeded in 1536-well plates pre-spotted with a 1:3 serial dilution of compound starting from 10 μM and incubated for 5 days. The cell viability was measured using the Cell Titer-Glo Luminescent Cell Viability Assay Kit (Promega) and read on an Envision (PerkinElmer) plate reader. The IC_{50} values were calculated from dose–response curves generated in GraphPad PRISM using a nonlinear regression four-parameter curve fitting model.

■ ASSOCIATED CONTENT

Supporting Information

The Supporting Information is available free of charge at https://pubs.acs.org/doi/10.1021/acs.jmedchem.0c02152.

LONP1 biochemical characterization, MD simulations, binding site dynamics of both LONP1 and 20S proteasome subunits, cell PD experiments, docking models, crystallographic conditions, and HPLC traces of **9d**, **12d**, and **14** (PDF)

9a Docking model in LONP1 (PDB)

9a Docking model in the β5-subunit of the 20S proteasome (PDB)

11d Docking model in the expanded pocket of the β5-subunit of 20S proteasome (PDB)

12d Docking model in the expanded pocket of the β5-subunit of the 20S proteasome (PDB)

Molecular formula strings (CSV)

Accession Codes

The authors will release the atomic coordinates and experimental data upon article publication. The crystallographic coordinates and structure factors have been deposited in the Protein Data Bank, www.pdb.org [PDB ID codes 6WYS (apo LONP1), 6X27 (bortezomib co-structure with LONP1), 6WZV (**9a** co-structure with LONP1), and 6X1M (**12d** co-structure with LONP1)].

■ AUTHOR INFORMATION

Corresponding Authors

Laura J. Kingsley − *Genomics Institute of the Novartis Research Foundation, San Diego, California 92121, United States*; Phone: +1-628-444-7236; Email: laura.kingsley@merck.com

Gérald Lelais − *Genomics Institute of the Novartis Research Foundation, San Diego, California 92121, United States*; orcid.org/0000-0002-6213-9863; Phone: +1-858-332-4452; Email: glelais@gnf.org

Authors

Xiaohui He − *Genomics Institute of the Novartis Research Foundation, San Diego, California 92121, United States*; orcid.org/0000-0003-1003-2631

Matthew McNeill − *Genomics Institute of the Novartis Research Foundation, San Diego, California 92121, United States*

John Nelson − *Genomics Institute of the Novartis Research Foundation, San Diego, California 92121, United States*

Victor Nikulin − *Genomics Institute of the Novartis Research Foundation, San Diego, California 92121, United States*

Zhiwei Ma − *Genomics Institute of the Novartis Research Foundation, San Diego, California 92121, United States*

Wenshuo Lu − *Genomics Institute of the Novartis Research Foundation, San Diego, California 92121, United States*

Vicki W. Zhou − *Genomics Institute of the Novartis Research Foundation, San Diego, California 92121, United States*

Mari Manuia − *Genomics Institute of the Novartis Research Foundation, San Diego, California 92121, United States*

Andreas Kreusch − *Genomics Institute of the Novartis Research Foundation, San Diego, California 92121, United States*

Mu-Yun Gao − *Genomics Institute of the Novartis Research Foundation, San Diego, California 92121, United States*

Darbi Witmer − *Genomics Institute of the Novartis Research Foundation, San Diego, California 92121, United States*

Mei-Ting Vaillancourt − *Genomics Institute of the Novartis Research Foundation, San Diego, California 92121, United States*

Min Lu − *Genomics Institute of the Novartis Research Foundation, San Diego, California 92121, United States*

Sarah Greenblatt − *Genomics Institute of the Novartis Research Foundation, San Diego, California 92121, United States*

Christian Lee − *Genomics Institute of the Novartis Research Foundation, San Diego, California 92121, United States*

Ajay Vashisht − *Genomics Institute of the Novartis Research Foundation, San Diego, California 92121, United States*

Steven Bender − *Genomics Institute of the Novartis Research Foundation, San Diego, California 92121, United States*

Glen Spraggon − *Genomics Institute of the Novartis Research Foundation, San Diego, California 92121, United States*

https://doi.org/10.1021/acs.jmedchem.0c02152
J. Med. Chem. 2021, 64, 4857−4869

Pierre-Yves Michellys − *Genomics Institute of the Novartis Research Foundation, San Diego, California 92121, United States*
Yong Jia − *Genomics Institute of the Novartis Research Foundation, San Diego, California 92121, United States*
Jacob R. Haling − *Genomics Institute of the Novartis Research Foundation, San Diego, California 92121, United States*

Complete contact information is available at: https://pubs.acs.org/10.1021/acs.jmedchem.0c02152

Author Contributions

The manuscript was written through contributions of all authors. All authors have given approval to the final version of the manuscript.

Notes

The authors declare no competing financial interest.

■ ACKNOWLEDGMENTS

The authors would like to thank all the supporting functions including Kimberly Sasher and her team (compound management), Thomas Hollenbeck and his team (analytical group) and Xiaoqi Gao (assay development).

■ ABBREVIATIONS

AAA+, ATPase associated with diverse cellular activities; AMP-PNP, adenylyl-imidodiphosphate; ATP, adenosine triphosphate; HTS, high-throughput screening; LONP1, Lon peptidase 1, mitochondrial; PD, pharmacodynamic

■ REFERENCES

(1) Sauer, R. T.; Baker, T. A. AAA+ proteases: ATP-fueled machines of protein destruction. *Annu. Rev. Biochem.* **2011**, *80*, 587−612.
(2) Olivares, A. O.; Baker, T. A.; Sauer, R. T. Mechanistic insights into bacterial AAA+ proteases and protein-remodelling machines. *Nat. Rev. Microbiol.* **2016**, *14*, 33−44.
(3) Bota, D. A.; Davies, K. J. A. Lon protease preferentially degrades oxidized mitochondrial aconitase by an ATP-stimulated mechanism. *Nat. Cell Biol.* **2002**, *4*, 674−680.
(4) Wong, K. S.; Houry, W. A. Recent Advances in Targeting Human Mitochondrial AAA+ Proteases to Develop Novel Cancer Therapeutics. In *Mitochondria in Health and in Sickness*; Urbani, A., Babu, M., Eds.; Springer Singapore: Singapore, 2019; pp 119−142.
(5) Glynn, S. E. Multifunctional mitochondrial AAA proteases. *Front. Mol. Biosci.* **2017**, *4*, 34.
(6) Kereïche, S.; Kovácik, L.; Bednár, J.; Pevala, V.; Kunová, N.; Ondrovicová, G.; Bauer, J.; Ambro, L.; Bellová, J.; Kutejová, E.; Raska, I. The N-terminal domain plays a crucial role in the structure of a full-length human mitochondrial Lon protease. *Sci. Rep.* **2016**, *6*, 33631.
(7) Snider, J.; Thibault, G.; Houry, W. A. The AAA+ superfamily of functionally diverse proteins. *Genome Biol.* **2008**, *9*, 216.
(8) Lin, C.-C.; Su, S.-C.; Su, M.-Y.; Liang, P.-H.; Feng, C.-C.; Wu, S.-H.; Chang, C.-I. Structural insights into the allosteric operation of the Lon AAA+ protease. *Structure* **2016**, *24*, 667−675.
(9) Su, S.-C.; Lin, C.-C.; Tai, H.-C.; Chang, M.-Y.; Ho, M.-R.; Babu, C. S.; Liao, J.-H.; Wu, S.-H.; Chang, Y.-C.; Lim, C.; Chang, C.-I. Structural basis for the magnesium-dependent activation and hexamerization of the Lon AAA+ protease. *Structure* **2016**, *24*, 676−686.
(10) Nishii, W.; Kukimoto-Niino, M.; Terada, T.; Shirouzu, M.; Muramatsu, T.; Kojima, M.; Kihara, H.; Yokoyama, S. A redox switch shapes the Lon protease exit pore to facultatively regulate proteolysis. *Nat. Chem. Biol.* **2015**, *11*, 46−51.
(11) Dikoglu, E.; Alfaiz, A.; Gorna, M.; Bertola, D.; Chae, J. H.; Cho, T.-J.; Derbent, M.; Alanay, Y.; Guran, T.; Kim, O.-H.; Llerenar Jr, J. C., Jr.; Yamamoto, G.; Superti-Furga, G.; Reymond, A.; Xenarios, I.; Stevenson, B.; Campos-Xavier, B.; Bonafé, L.; Superti-Furga, A.; Unger, S. Mutations in LONP1, a mitochondrial matrix protease, cause CODAS syndrome. *Am. J. Med. Genet., Part A* **2015**, *167*, 1501−1509.
(12) Peter, B.; Waddington, C. L.; Oláhová, M.; Sommerville, E. W.; Hopton, S.; Pyle, A.; Champion, M.; Ohlson, M.; Siibak, T.; Chrzanowska-Lightowlers, Z. M. A.; Taylor, R. W.; Falkenberg, M.; Lightowlers, R. N. Defective mitochondrial protease LonP1 can cause classical mitochondrial disease. *Hum. Mol. Genet.* **2018**, *27*, 1743−1753.
(13) Nie, X.; Li, M.; Lu, B.; Zhang, Y.; Lan, L.; Chen, L.; Lu, J. Down-regulating overexpressed human Lon in cervical cancer suppresses cell proliferation and bioenergetics. *PLoS One* **2013**, *8*, No. e81084.
(14) Quirós, P. M.; Español, Y.; Acín-Pérez, R.; Rodríguez, F.; Bárcena, C.; Watanabe, K.; Calvo, E.; Loureiro, M.; Fernández-García, M. S.; Fueyo, A.; Vázquez, J.; Enríquez, J. A.; López-Otín, C. ATP-dependent Lon protease controls tumor bioenergetics by reprogramming mitochondrial activity. *Cell Rep.* **2014**, *8*, 542−556.
(15) Pinti, M.; Gibellini, L.; Nasi, M.; De Biasi, S.; Bortolotti, C. A.; Iannone, A.; Cossarizza, A. Emerging role of Lon protease as a master regulator of mitochondrial functions. *Biochim. Biophys. Acta* **2016**, *1857*, 1300−1306.
(16) Lu, B.; Lee, J.; Nie, X.; Li, M.; Morozov, Y. I.; Venkatesh, S.; Bogenhagen, D. F.; Temiakov, D.; Suzuki, C. K. Phosphorylation of human TFAM in mitochondria impairs DNA binding and promotes degradation by the AAA+ Lon protease. *Mol. Cell* **2013**, *49*, 121−132.
(17) Key, J.; Kohli, A.; Bárcena, C.; López-Otín, C.; Heidler, J.; Wittig, I.; Auburger, G. Global proteome of LonP1+/− mouse embryonal fibroblasts reveals impact on respiratory chain, but no interdependence between eral1 and mitoribosomes. *Int. J. Mol. Sci.* **2019**, *20*, 4523.
(18) Gibellini, L.; Losi, L.; De Biasi, S.; Nasi, M.; Lo Tartaro, D.; Pecorini, S.; Patergnani, S.; Pinton, P.; De Gaetano, A.; Carnevale, G.; Pisciotta, A.; Mariani, F.; Roncucci, L.; Iannone, A.; Cossarizza, A.; Pinti, M. LonP1 differently modulates mitochondrial function and bioenergetics of primary versus metastatic colon cancer cells. *Front. Oncol.* **2018**, *8*, 254.
(19) Weiss, W. A.; Taylor, S. S.; Shokat, K. M. Recognizing and exploiting differences between RNAi and small-molecule inhibitors. *Nat. Chem. Biol.* **2007**, *3*, 739−744.
(20) Carter, A. J.; Kraemer, O.; Zwick, M.; Mueller-Fahrnow, A.; Arrowsmith, C. H.; Edwards, A. M. Target 2035: probing the human proteome. *Drug Discovery Today* **2019**, *24*, 2111−2115.
(21) Van Melderen, L.; Aertsen, A. Regulation and quality control by Lon-dependent proteolysis. *Res. Microbiol.* **2009**, *160*, 645−651.
(22) Fishovitz, J.; Li, M.; Frase, H.; Hudak, J.; Craig, S.; Ko, K.; Berdis, A. J.; Suzuki, C. K.; Lee, I. Active-site-directed chemical tools for profiling mitochondrial Lon protease. *ACS Chem. Biol.* **2011**, *6*, 781−788.
(23) Csizmadia, V.; Hales, P.; Tsu, C.; Ma, J.; Chen, J.; Shah, P.; Fleming, P.; Senn, J. J.; Kadambi, V. J.; Dick, L.; Wolenski, F. S. Proteasome inhibitors bortezomib and carfilzomib used for the treatment of multiple myeloma do not inhibit the serine protease HtrA2/Omi. *Toxicol. Res.* **2016**, *5*, 1619−1628.
(24) Liao, J.-H.; Ihara, K.; Kuo, C.-I.; Huang, K.-F.; Wakatsuki, S.; Wu, S.-H.; Chang, C.-I. Structures of an ATP-independent Lon-like protease and its complexes with covalent inhibitors. *Acta Crystallogr., Sect. D: Struct. Biol.* **2013**, *69*, 1395−1402.
(25) Kupperman, E.; Lee, E. C.; Cao, Y.; Bannerman, B.; Fitzgerald, M.; Berger, A.; Yu, J.; Yang, Y.; Hales, P.; Bruzzese, F.; Liu, J.; Blank, J.; Garcia, K.; Tsu, C.; Dick, L.; Fleming, P.; Yu, L.; Manfredi, M.; Rolfe, M.; Bolen, J. Evaluation of the proteasome inhibitor MLN9708 in preclinical models of human cancer. *Cancer Res.* **2010**, *70*, 1970−1980.
(26) Adams, J.; Behnke, M.; Chen, S.; Cruickshank, A. A.; Dick, L. R.; Grenier, L.; Klunder, J. M.; Ma, Y.-T.; Plamondon, L.; Stein, R. L. Potent and selective inhibitors of the proteasome: dipeptidyl boronic acids. *Bioorg. Med. Chem. Lett.* **1998**, *8*, 333−338.

(27) Adams, J.; Ma, Y.-T.; Stein, R.; Baevsky, M.; Grenier, L.; Plamondon, L. Boronic Ester and Acid Compounds. U.S. Patent 5,780,454 A, 1995.
(28) Ivanov, A. S.; Zhalnina, A. A.; Shishkov, S. V. A convergent approach to synthesis of bortezomib: the use of TBTU suppresses racemization in the fragment condensation. *Tetrahedron* **2009**, *65*, 7105−7108.
(29) Matteson, D. S.; Sadhu, K. M. Boronic ester homologation with 99% chiral selectivity and its use in syntheses of the insect pheromones (3S,4S)-4-methyl-3-heptanol and exo-brevicomin. *J. Am. Chem. Soc.* **1983**, *105*, 2077−2078.
(30) Matteson, D. S.; Jesthi, P. K.; Sadhu, K. M. Synthesis and properties of pinanediol alpha-amido boronic esters. *Organometallics* **1984**, *3*, 1284−1288.
(31) Matteson, D. S. Alpha-halo boronic esters - intermediates for stereodirected synthesis. *Chem. Rev.* **1989**, *89*, 1535−1551.
(32) Buesking, A. W.; Bacauanu, V.; Cai, I.; Ellman, J. A. Asymmetric synthesis of protected alpha-amino boronic acid derivatives with an air- and moisture-stable Cu(II) catalyst. *J. Org. Chem.* **2014**, *79*, 3671−3677.
(33) Schrader, J.; Henneberg, F.; Mata, R. A.; Tittmann, K.; Schneider, T. R.; Stark, H.; Bourenkov, G.; Chari, A. The inhibition mechanism of human 20S proteasomes enables next-generation inhibitor design. *Science* **2016**, *353*, 594−598.
(34) Groll, M.; Berkers, C. R.; Ploegh, H. L.; Ovaa, H. Crystal structure of the boronic acid-based proteasome inhibitor bortezomib in complex with the yeast 20S proteasome. *Structure* **2006**, *14*, 451−456.
(35) Diaz, D. B.; Yudin, A. K. The versatility of boron in biological target engagement. *Nat. Chem.* **2017**, *9*, 731−742.
(36) McDonald, E. R.; de Weck, A.; Schlabach, M. R.; Billy, E.; Mavrakis, K. J.; Hoffman, G. R.; Belur, D.; Castelletti, D.; Frias, E.; Gampa, K.; Golji, J.; Kao, I.; Li, L.; Megel, P.; Perkins, T. A.; Ramadan, N.; Ruddy, D. A.; Silver, S. J.; Sovath, S.; Stump, M.; Weber, O.; Widmer, R.; Yu, J.; Yu, K.; Yue, Y.; Abramowski, D.; Ackley, E.; Barrett, R.; Berger, J.; Bernard, J. L.; Billig, R.; Brachmann, S. M.; Buxton, F.; Caothien, R.; Caushi, J. X.; Chung, F. S.; Cortés-Cros, M.; deBeaumont, R. S.; Delaunay, C.; Desplat, A.; Duong, W.; Dwoske, D. A.; Eldridge, R. S.; Farsidjani, A.; Feng, F.; Feng, J.; Flemming, D.; Forrester, W.; Galli, G. G.; Gao, Z.; Gauter, F.; Gibaja, V.; Haas, K.; Hattenberger, M.; Hood, T.; Hurov, K. E.; Jagani, Z.; Jenal, M.; Johnson, J. A.; Jones, M. D.; Kapoor, A.; Korn, J.; Liu, J.; Liu, Q.; Liu, S.; Liu, Y.; Loo, A. T.; Macchi, K. J.; Martin, T.; McAllister, G.; Meyer, A.; Mollé, S.; Pagliarini, R. A.; Phadke, T.; Repko, B.; Schouwey, T.; Shanahan, F.; Shen, Q.; Stamm, C.; Stephan, C.; Stucke, V. M.; Tiedt, R.; Varadarajan, M.; Venkatesan, K.; Vitari, A. C.; Wallroth, M.; Weiler, J.; Zhang, J.; Mickanin, C.; Myer, V. E.; Porter, J. A.; Lai, A.; Bitter, H.; Lees, E.; Keen, N.; Kauffmann, A.; Stegmeier, F.; Hofmann, F.; Schmelzle, T.; Sellers, W. R. Project DRIVE: a compendium of cancer dependencies and synthetic lethal relationships uncovered by large-scale, deep RNAi screening. *Cell* **2017**, *170*, 577−592.
(37) Barretina, J.; Caponigro, G.; Stransky, N.; Venkatesan, K.; Margolin, A. A.; Kim, S.; Wilson, C. J.; Lehár, J.; Kryukov, G. V.; Sonkin, D.; Reddy, A.; Liu, M.; Murray, L.; Berger, M. F.; Monahan, J. E.; Morais, P.; Meltzer, J.; Korejwa, A.; Jané-Valbuena, J.; Mapa, F. A.; Thibault, J.; Bric-Furlong, E.; Raman, P.; Shipway, A.; Engels, I. H.; Cheng, J.; Yu, G. K.; Yu, J.; Aspesi, P., Jr.; de Silva, M.; Jagtap, K.; Jones, M. D.; Wang, L.; Hatton, C.; Palescandolo, E.; Gupta, S.; Mahan, S.; Sougnez, C.; Onofrio, R. C.; Liefeld, T.; MacConaill, L.; Winckler, W.; Reich, M.; Li, N.; Mesirov, J. P.; Gabriel, S. B.; Getz, G.; Ardlie, K.; Chan, V.; Myer, V. E.; Weber, B. L.; Porter, J.; Warmuth, M.; Finan, P.; Harris, J. L.; Meyerson, M.; Golub, T. R.; Morrissey, M. P.; Sellers, W. R.; Schlegel, R.; Garraway, L. A. The cancer cell line encyclopedia enables predictive modelling of anticancer drug sensitivity. *Nature* **2012**, *483*, 603−607.

https://doi.org/10.1021/acs.jmedchem.0c02152
J. Med. Chem. 2021, 64, 4857−4869